NACA

RESEARCH MEMORANDUM

FREE-FLIGHT DETERMINATION OF BOUNDARY-LAYER TRANSITION AND HEAT TRANSFER FOR A HEMISPHERE-CYLINDER AT MACH NUMBERS TO 5.6

By M. J. Krasnican and R. J. Wisniewski

Lewis Flight Propulsion Laboratory
Cleveland, Ohio

NATIONAL ADVISORY COMMITTEE FOR AERONAUTICS

WASHINGTON

October 21, 1957

[redacted]

NATIONAL ADVISORY COMMITTEE FOR AERONAUTICS

RESEARCH MEMORANDUM

FREE-FLIGHT DETERMINATION OF BOUNDARY-LAYER TRANSITION AND HEAT TRANSFER FOR A HEMISPHERE-CYLINDER AT MACH NUMBERS TO 5.6

By M. J. Krasnican and R. J. Wisniewski

SUMMARY

A highly polished, 9-inch-diameter hemisphere-cylinder has been flown to obtain boundary-layer transition and heat-transfer data. The free-flight test model was launched 30° downward from an aircraft at an altitude of 25,400 feet and reached a maximum Mach number of 5.59 at an altitude of 13,450 feet. The maximum free-stream Reynolds number based on body diameter was 19.9×10^6.

Turbulent flow was observed at all stations aft of the 11.5° hemisphere station. The transition Reynolds number based on momentum thickness was found to be less than 144 at a free-stream Mach number of 2.07 and less than 192 at a free-stream Mach number of 5.48. A peak heating rate of 489 Btu/(sq ft)(sec) was determined at the 22.75° hemisphere station.

Experimental Stanton numbers at the stagnation point were in good agreement with theory. At the 11.5° and 22.75° hemisphere stations, experimental Stanton numbers were in accord with turbulent theory. Stanton numbers at the 34°, 57°, 69°, and 81° hemisphere stations generally fell below turbulent theory. On the cylinder, turbulent theory and experimental Stanton number were in close agreement.

INTRODUCTION

Aerodynamic heating on a hypersonic vehicle during atmospheric reentry presents a number of difficulties to the designer. In order to estimate the amount of heating a vehicle will have to sustain, a knowledge of the expected transition position is required. For example, transition occurring in the subsonic region of a blunt body could increase the heating rates in this region to three or four times the stagnation-point heating rate.

Flight and wind tunnel transition data (refs. 1 to 6) on slender bodies have shown that large delays of transition are possible with moderate cooling. However, for hypersonic atmospheric reentry slender bodies offer low heat capacity at the tip and limited space for the installation of internal cooling devices. Thus, high-drag bodies which possess larger heat capacity and greater space for internal cooling devices have become of interest. In addition, under the same reentry conditions, high-drag bodies will sustain less total heating than slender, low-drag vehicles when their boundary-layer states are the same, laminar or turbulent (ref. 7).

Recent investigations on hemisphere-cylinders and other blunt bodies (refs. 8 to 13) have indicated that the large delays in transition observed on slender bodies may not be possible on blunt bodies. At present no clear understanding of this phenomenon is available.

This flight investigation presents transition data on a hemisphere-cylinder at high Reynolds numbers and hypersonic Mach numbers. In the determination of transition, heat-transfer data have also been obtained which offer a comparison with available theory.

SYMBOLS

a_n	axial acceleration, g's
b	semihemispherical arc length, ft
c_p	specific heat of air at constant pressure
$c_{p,s}$	specific heat of skin
D	body diameter, ft
d_s	thickness of skin, ft
F	thrust, lb
g	acceleration due to gravity, ft/sec^2
h	convective heat-transfer coefficient, $Btu/(sq\ ft)(sec)(^oF)$
k	roughness height, microin.
M	Mach number
Pr	Prandtl number, $\frac{c_p\mu}{\kappa}$

p static pressure, lb/sq ft

q heat-transfer rate, Btu/(sq ft)(sec)

Re Reynolds number

$\tilde{Re}$ integrated Reynolds number, $\dfrac{\int_0^x \rho_l \mu_l V_l r_0^2 \, dx}{\mu_l^2 r_0^2}$

$Re_{l,D}$ Reynolds number based on body diameter and free-stream conditions, $\dfrac{\rho_l V_l D}{\mu_l}$

Re_l Reynolds number based on local flow conditions and total length of run, $\dfrac{\rho_l V_l x}{\mu_l}$

Re_θ Reynolds number based on local flow conditions and momentum thickness, $\dfrac{\rho_l V_l \theta}{\mu_l}$

r_0 radius from axis of revolution to body surface, ft

St Stanton number, $\dfrac{h}{c_{p,l}\rho_l V_l}$

T total temperature, $^\circ R$

t static temperature, $^\circ R$

V velocity, ft/sec

x distance along surface, measured from stagnation point in meridional plane, ft

z altitude, ft

α angle on a sphere between stagnation point and a given station, deg

β circumferential angle (or generator) with respect to reference shown in fig. 2, deg

η recovery factor

θ momentum thickness, microin. $\int_0^\delta \dfrac{\rho V}{\rho_l V_l}\left(1 - \dfrac{V}{V_l}\right)dy$

$\varkappa$ thermal conductivity

μ absolute viscosity, (lb-sec)/sq ft

ρ density, $(\text{lb-sec}^2)/\text{ft}^4$

τ time, sec

[redacted]

Subscripts:

aw	adiabatic wall
G	material
l	local condition just outside boundary layer
tr	condition at transition
t_2	stagnation condition behind normal shock
w	body surface condition
1	free-stream conditions ahead of shock
2	conditions behind normal shock

APPARATUS AND PROCEDURE

Test Vehicle

The test vehicle consisted of a highly polished hemisphere-cylinder with a rocket-motor afterbody. The maximum body diameter was 9.00 inches. Pertinent physical dimensions of the air-launched rocket configuration are shown in figure 1, while table I lists additional data on the test body. The location of thermocouples and pressure taps is presented in figure 2. In order to connect the polished nose shell to the rocket-motor afterbody, a cylindrical coupling was utilized. This intermediate section also served to house flush slot antenna plates made of Inconel and to support the telemeter assembly within the nose section (fig. 3).

Commercially pure nickel was used to fabricate the polished forebody skin which was 0.062 inch (nominal) thick. The actual skin thickness for each thermocouple station and the wetted surface distance to each station (from stagnation point) are shown in table II. (Thickness measurements are estimated to be within $\pm$0.0005 in.) An industrial diamond paste was used to secure a surface finish of 3 to 5 microinches in the vicinity of the stagnation region and 5 microinches aft of the stagnation region (on the polished hemisphere-cylinder forebody). It is estimated that scratches of the order of 15 microinches existed aft of the stagnation region. These values of roughness were measured by an interferometer on a sample of nickel polished in a manner similar to that used on the polished nose section.

Since no instrumentation was aft of 18.47 inches (axial distance), no effort was made to improve the surface finish of the coupling cover plates and the rocket-motor body. Figure 4 illustrates the completed test vehicle. At the missile rear, a cruciform fin assembly (consisting of a cylindrical collar and four fins) was connected to the rocket motor to provide aerodynamic stability. The fins were fabricated from mild steel (3/16-in. sheet) and had a total span of 28.68 inches and a root chord of 13.50 inches. The leading edges of the fins were tapered and rounded to a 1/32-inch radius. Table III gives the general specifications and rated performance of the T-64 rocket at sea level as obtained from reference 14.

Methods of Measurement

A radio telemeter transmitter was used to send data to ground receiving stations. This telemeter assembly was housed in the volume enclosed by the polished hemisphere-cylinder.

Temperature measurements at 12 stations were telemetered on two channels, each of which was switched (electrical commutation) to record six temperature stations at intervals of about 0.15 second. A built-in calibration system permitted a cyclic temperature calibration (0, 1/2, and full scale) to be recorded about every 0.30 second. All the thermocouples were 28-gauge Chromel-Alumel wire and were located in the same meridian except stations C and E (fig. 2). Each wire was coated with a high-temperature paint which was furnace-fired to yield a ceramic coating of several thousandths of an inch. The two inside skin thermocouples (stations C and G, fig. 2) were spotwelded to the inside skin surface. All other thermocouples were installed as follows: the hemisphere-cylinder was drilled with two small, adjacent holes at a given station to permit the thermocouple wires to protrude just outside the exterior surface where the thermocouple junction was made. A heliarc-type weld fused the junction to the exterior surface which formed a weld approximately 0.25 inch in diameter. This weld was ground flush with the outer-skin surface and polished. Upon examination of a cross section of a sample weld made in the above manner, the depth of weld penetration was about 0.015 inch. For purposes of analysis, the assumption was made that all outside thermocouples were located within 0.015 inch of the exterior surface. It was estimated that the minimum and maximum depths of weld penetration were 0.005 and 0.020 inch, respectively. The maximum probable error in measuring skin temperatures was estimated to be within ±2 percent of the full-scale range of instruments.

In addition, continuous measurements were recorded from two axial accelerometers and four pressure taps. These orifices were located

11.25°, 45°, and 69° from the stagnation point and at cylinder station P (fig. 2), 2.14 diameters behind the hemisphere-cylinder junction. The type and ranges of the instrumentation are as follows:

Quantity	Range	Station (fig. 2)
Axial acceleration, g's	1 to -90	-
Axial acceleration, g's	0 to 135	-
Skin temperature (thermocouple), °R	400 to 1800	D,E,F,G,H,I
Skin temperature (thermocouple), °R	400 to 1200	A,B,C,J,K,L
Cylinder static pressure, lb/sq in. abs	1 to 15	P
69° Nose static pressure, lb/sq in. abs	4 to 125	Q
45° Nose static pressure, lb/sq in. abs	4 to 250	N
11.25° Nose static pressure, lb/sq in. abs	4 to 425	M

The diameter of the pressure orifices was 0.067 inch. At the cylinder pressure station P a bellows-type pressure capsule was employed while the pressure taps on the hemisphere were connected to bourdon-type transducers.

Prior to flight, a soft-paper, hemispherical mask was placed over the polished hemisphere to prevent possible erosion of the nose surface before missile drop. The top of the paper mask was connected to the plane by a lightweight string which was interlaced in the mask to ensure complete separation from the missile nose as soon as the missile drop occurred (fig. 5).

The test vehicle was carried aloft by the F2H-2B aircraft shown in figure 5. The model was launched over Wallops Island, Virginia 30° downward at an altitude of 25,400 feet. A time-delay box containing delay squibs permitted an ignition delay of 14.76 seconds from launch, after which ignition took place at an altitude of 17,720 feet. Tracking of the missile was accomplished from launch to about 1 second after ignition by means of ground radar and phototheodolite equipment. Following this

time, missile velocity exceeded the tracking speed of the aforesaid ground apparatus.

Variation of ambient pressure and temperature with altitude was determined from a Rawinsonde survey made immediately following the flight.

Calculation Procedure

Free-stream velocity was based on a faired curve derived from radar measurements at the first part of the flight (up to 14.32 sec) and from an integration of the total acceleration for the latter part of the flight.

Local heat-transfer coefficients were found from the equation

$$\rho_G c_{p,s} d_s \frac{dt_w}{d\tau} = h(t_{aw} - t_w) \tag{1}$$

Equation (1) implies that the losses due to conduction and radiation are small. The maximum error due to conduction through the skin is 7 percent of the convective heat input, while the maximum loss due to conduction along the skin is less than 1 percent of convective heat input. Radiation losses are negligible, which makes the maximum total error due to conduction 8 percent of the convective heat input. The adiabatic wall temperature was calculated from the equation

$$t_{aw} = t_l + \eta(T_{t_2} - t_l) \tag{2}$$

The recovery factor was calculated by using $Pr^{1/3}$ (turbulent flow) evaluated at the local temperature. A recovery factor of 1 is used for stagnation-point calculations.

The local pressure on the hemisphere was found by using the Newtonian pressure distribution. The local static pressure on the cylinder was assumed to be equal to the free-stream static pressure, and the total pressure was the same as that behind the bow shock. All other local external conditions were found by assuming the total pressure behind the normal shock and applying the conservation of energy and the equation of state. The properties of air were evaluated from references 15 and 16.

Although the thermocouple installations were estimated to be from 0.005 to 0.020 inch below the surface, the error in assuming the measured temperatures to exist on the wall is negligible. The raw temperature data were faired, and slopes of temperature against time were found by using the five-point numerical differentiation given in reference 17.

[redacted]

The specific heat curve of nickel was obtained from figure 7 (p. 16) of reference 18. A discontinuity in this curve exists in the temperature range encountered in the latter portion of the flight.

RESULTS AND DISCUSSION

Data were obtained for the test vehicle for 16.34 seconds of the flight. The telemeter signal terminated at the end of this period. Time histories of the axial acceleration (exclusive of gravity) and the free-stream velocity are presented in figure 6. At 14.76 seconds (rocket ignition), the velocity was 914 feet per second. Peak velocity was attained at 16.34 seconds and had a value of 6020 feet per second. A maximum acceleration of 110.6 g's was recorded at 15.68 seconds. The optical tracking facilities of the radar unit failed to maintain contact with the test vehicle after 14.82 seconds, and no ground-tracking data were obtained thereafter.

A comparison of the T-64 rocket thrust at sea level (11-in. nozzle) with calculated thrust during flight (9-in. nozzle) is shown in figure 7. Computed thrust was based on measured rocket acceleration, assumed fuel consumption (function of measured rocket acceleration), and calculated drag. The thrust curve indicates that the rocket was near the end of its thrust schedule at 16.34 seconds.

Free-Stream Conditions

The time histories of the following free-stream conditions are presented in figure 8: (a) altitude, (b) static pressure, (c) static temperature, (d) total temperature, (e) Reynolds number per foot, (f) Mach number, and (g) Reynolds number (based on body diameter). The maximum total temperature of 3160° R (fig. 8(d)) occurred at 16.34 seconds.

The free-stream Reynolds number per foot (fig. 8(e)) was a maximum of 26.5×10^6 at 16.34 seconds and gave a maximum free-stream Reynolds number of 270.5×10^6 based on a model length of 10.22 feet. Based on body diameter, the maximum free-stream Reynolds number (fig. 8(g)) was 19.9×10^6. The free-stream Mach number (fig. 8(f)) reached a maximum of 5.59 at an altitude of 13,450 feet.

Pressure Measurements

Figure 9 illustrates the longitudinal pressure coefficient distribution at a peak Mach number of 5.59 at the 11.25°, 45°, and cylinder

pressure taps. Comparison is also made with Newtonian theory

$$\frac{p - p_1}{p_{t_2} - p_1} = \cos^2 \alpha \tag{3}$$

and comparable experimental results (refs. 19 and 20).

No data are presented for the 69° pressure tap since the telemeter record revealed that this transducer was apparently sticking until the model reached the peak Mach number range. The ratio of local to free-stream static pressure plotted against free-stream Mach number is presented in figure 10 for the 11.25° and 45° stations during the high Mach number portion of the flight. In addition, comparison is made with the $\cos^2 \alpha$ law.

The peak free-stream Mach number calculated from the pressure ratio at the 11.25° station agrees within 1 percent with the free-stream Mach number determined by radar and accelerometer integration. When the local pressure at the 45° station is compared with the total pressure (at 16.34 sec), the local Mach number at this station is very close to Mach 1, which indicates that the sonic point on the body was near the 45° station.

Temperature Measurements

Faired time histories of the temperature data are presented in figure 11 together with experimental points. All temperatures presented in this figure are the measured outside wall temperatures with the exception of stations 11.5° and 46.5°, where inside wall temperatures are presented. Figure 11(a) presents both the inside and outside wall temperature for the same surface distance (11.5°), but at slightly different generator positions ($\Delta\beta = 32°$ corresponding to a surface distance of 1/2 in.). The measured inside temperature of the 11.5° station indicates a large drop through the skin early in time. Calculations of inside temperature based on measured outside temperature and using the method of reference 21 are also presented. The theoretical calculation agrees quite closely at times after 15.9 seconds but does not predict the large measured drop through the skin which occurred early in the flight. Some limited past experience and the above calculations indicate that the method of installation of the inner thermocouple may be inadequate.

The maximum temperature and the maximum temperature rise with time on the 180° generator ($\beta = 180°$) occurred at the 22.75° station (fig. 11(c)). A maximum temperature of 1227° R and a maximum temperature rise of 1347° R per second were measured at the termination of the flight. Temperatures at the 34° station were lower than those at the 22.75°

[redacted]

station. The maximum temperature recorded during the flight occurred at the 45° station on the 0° generator (fig. 11(d)). However, scatter of the data prevented an accurate faired temperature history for this station.

Heat-Transfer Measurement

The experimental heat-transfer data are presented in figure 12 in the form of Stanton numbers based on free-stream conditions. Also shown are the laminar stagnation point, turbulent sphere, and turbulent flat plate theory of Van Driest (ref. 22). After 15.6 seconds, good agreement with laminar theory has been obtained at the stagnation point of the hemisphere. Measurements made on the hemisphere at the 11.5° ($x/b = 0.127$) and 22.75° ($x/b = 0.253$) stations agree closely with turbulent theory. Measurements at the 57° ($x/b = 0.635$), 69° ($x/b = 0.767$), and 81° ($x/b = 0.902$) stations fall below theory. However, some disagreement might be expected as the blunt body turbulent theory of Van Driest does not take into account the effects of compressibility.

The data of the 34° ($x/b = 0.379$) station show poor agreement with theory and in many cases are of the same order of magnitude as those of the 57° station. The apparent disagreement of the 34° station data with theory and the fair agreement of the other hemisphere stations raise some question as to the validity of the 34° station data. One possible explanation for the low measured heating rates of the 34° station is that the thermocouple leads short-circuited to the inner surface of the shell. In this case, the thermocouple would read less than the outer-surface temperature, and a lower-than-actual heating rate would be indicated.

The data obtained at 1.47 ($x/b = 1.209$) and 22.22 ($x/b = 2.730$) inches from the hemisphere-cylinder junction show good agreement with the turbulent flat plate theory (ref. 22) when the free-stream static pressure is assumed to exist on the cylinder.

The experimental heating rates used to calculate Stanton numbers on the hemisphere and cylinder are presented in figure 13 for various times. The maximum heating rate occurs at the 22.75° station and has a value of 489 Btu/(sq ft)(sec) at 16.2 seconds and Mach number of 5.19. At 15.8 seconds the heating rate of the 22.75° station is 3.6 times the stagnation heating rate.

Transition and Transition Parameters

For the 180° generator, the heat-transfer coefficients have been shown to have a minimum value at the stagnation point and to increase in

a direction away from the stagnation point (fig. 12); these coefficients are in reasonable agreement with turbulent theory. Laminar theory, on the other hand, predicts a maximum heat-transfer rate at the stagnation point, with decreasing values away from the stagnation point. Consequently, if the flow were laminar, a decrease in surface temperature (at a given time) would be expected away from the stagnation point. But the surface temperature at the 11.5° station is always higher than the stagnation-point temperature (fig. 14). Therefore, it must be concluded that transition on the 180° generator occurred ahead of the 11.5° station.

A comparison of the temperature rise of the 11.5° station (180° generator) and the 45° station (0° generator) with the stagnation-point temperature rise indicates that transition did not occur simultaneously on both sides of the hemisphere. No laminar flow is observed at the 11.5° station after approximately 15.1 seconds, while laminar flow at the 45° station appears to exist to approximately 15.5 seconds.

The lack of instrumentation between the stagnation point and the 11.5° station makes it impossible to determine exactly the Reynolds number of transition on the 180° generator. The upper limits of the transition Reynolds number and several parameters considered in reference 9 as a means of correlating transition on blunt bodies are presented in table IV. Figure 15 is a plot of the integrated Reynolds number $\bar{R}e$ for various hemisphere locations as a function of time. Figure 16 presents the local Reynolds number and the wall-to-local temperature ratio (indication of the amount of boundary-layer cooling) for two conditions at which heat-transfer data have been presented.

The method of Cohen and Reshotko (ref. 23) was used to calculate the momentum thickness in the region of the stagnation point. The Reynolds number based on momentum thickness has been calculated using the method suggested in reference 9.

The Reynolds number of transition based on momentum thickness on the 180° generator was less than 144 at a Mach number of 2.07 and less than 192 at a Mach number of 5.48. As the Mach number increased from 2.07 to 5.48, Re_θ at the sonic point increased from 565 to 724. However, transition at the 45° station of the 0° generator did not occur until Re_θ at the sonic point was approximately 640.

According to the stability theory of Dunn and Lin (ref. 24), cooling can stabilize a supersonic boundary layer to large Reynolds numbers but has little effect on a subsonic boundary layer. This predicted delay of supersonic transition has been found on slender bodies with moderate cooling (refs. 1 to 6) as mentioned previously. We may hypothesize a similar transition behavior on a blunt body if the local Reynolds number at the sonic point does not exceed some critical value. If the local Reynolds number at the sonic point is small or below this critical value,

transition would occur in the region of supersonic external flow and, therefore, would be strongly influenced by cooling. However, when the local Reynolds number at the sonic point becomes large and exceeds a critical value, transition will occur in the region of subsonic external flow and would be little influenced by cooling. A rapid forward movement of transition from the supersonic region to the subsonic region would therefore be expected when the Reynolds number at the sonic point exceeds a certain critical value. Such rapid movements of transition have been observed in references 7 and 8 at sonic-point Reynolds numbers from 500 to 700.

Although cooling has little effect on stabilizing a subsonic boundary layer, it tends to thin the boundary layer. This effect, combined with the greater sensitivity of subsonic boundary layer to roughness, indicates that the critical sonic-point Reynolds number may be influenced quite strongly by surface roughness. In the present test the early transition observed on the 180° generator may be due to surface irregularities other than the 5-microinch surface roughness. Such surface irregularities may have been absent along the 0° generator, which would account for the later transition obtained along this generator.

Another proposed explanation for early transition is the destabilizing effect which centrifugal force and accelerated motion might have on a laminar boundary layer on a highly cooled curved surface. However, a recent paper by Lees (ref. 25) concludes that when the angular momentum is taken into account the criterion for dynamic stability is always satisfied for a highly cooled convex surface. It must also be pointed out that instability due to centrifugal forces cannot explain an unsymmetrical transition front as the centrifugal forces are the same on both sides of the hemisphere.

SUMMARY OF RESULTS

A highly polished, 9-inch-diameter hemisphere-cylinder was flown to obtain boundary-layer transition data and heat-transfer coefficients. The following results were obtained:

1. A maximum free-stream Mach number of 5.59 was attained at an altitude of 13,450 feet following a 30° downward launching from an F2H-2B airplane. The maximum free-stream Reynolds number based on body diameter was 19.9×10^6.

2. Early transition from laminar to turbulent flow was noted and occurred at or before the 11.5° hemisphere station on the 180° generator. Transition Reynolds number based on momentum thickness was less than 144 at a free-stream Mach number of 2.07 and less than 192 at a Mach number

of 5.48. A later asymmetric transition was observed on the 0° generator which may indicate that transition on the 180° generator was due to surface irregularities other than the nominal 5-microinch surface.

3. A peak heating rate of 489 Btu/(sq ft)(sec) was measured at the 22.75° station at a free-stream Mach number of 5.19. The maximum skin temperature was 1227° R and occurred at the 22.75° station at the time of flight termination (free-stream Mach number of 5.59 and free-stream Reynolds number per foot of 26.5×10^6).

4522

4. Good agreement was obtained between theoretical and experimental free-stream Stanton numbers at the stagnation point on the hemisphere. At the 11.5° and 22.75° hemisphere stations, experimental free-stream Stanton numbers were in good accord with turbulent theory. Experimental free-stream Stanton numbers at the 34°, 57°, 69°, and 81° stations generally fell somewhat below turbulent theory. On the cylinder, turbulent theory and experimental free-stream Stanton numbers were in good agreement.

Lewis Flight Propulsion Laboratory
National Advisory Committee for Aeronautics
Cleveland, Ohio, June 14, 1957

REFERENCES

1. Disher, John H., and Rabb, Leonard: Observation of Laminar Flow on a Blunted 15° Cone-Cylinder in Free Flight at High Reynolds Numbers and Free-Stream Mach Numbers to 8.17. NACA RM E56G23, 1956.

2. Rumsey, Charles B., and Lee, Dorothy B.: Measurements of Aerodynamic Heat Transfer and Boundary-Layer Transition on a 15° Cone in Free Flight at Supersonic Mach Numbers up to 5.2. NACA RM L56F26, 1956.

3. Rabb, Leonard, and Krasnican, Milan J.: Observation of Laminar Flow on an Air-Launched 15° Cone-Cylinder at Local Reynolds Numbers to 50×10^6 at Peak Mach Number of 6.75. NACA RM E56L03, 1957.

4. Merlet, Charles F., and Rumsey, Charles B.: Supersonic Free-Flight Measurement of Heat Transfer and Transition on a 10° Cone Having a Low Temperature Ratio. NACA RM L56L10, 1957.

5. Jack, John R., and Diaconis, N. S.: Variation of Boundary-Layer Transition with Heat Transfer on Two Bodies of Revolution at a Mach Number of 3.12. NACA TN 3562, 1955.

6. Diaconis, N. S., Jack, John R., and Wisniewski, Richard J.: Boundary-Layer Transition at Mach 3.12 as Affected by Cooling and Nose Blunting. NACA TN 3928, 1957.

7. Allen, H. Julian, and Eggers, A. J., Jr.: A Study of the Motion and Aerodynamic Heating of Missiles Entering the Earth's Atmosphere at High Supersonic Speeds. NACA RM A53D28, 1953.

8. Chauvin, Leo T.: Aerodynamic Heating of Aircraft Components. NACA RM L55L19b, 1956.

9. Denison, M. R., and Tellep, D. M.: X-17 - R-1 Preliminary Flight Report - Analysis of Transition and Aerodynamic Heating. MSD 1709, Missile Systems Div., Lockheed Aircraft Corp., May 8, 1956.

10. Garland, Benjamine J., and Chauvin, Leo T.: Measurements of Heat Transfer and Boundary-Layer Transition of an 8-Inch Diameter Hemisphere-Cylinder in Free Flight for a Mach Number Range of 2.00 to 3.88. NACA RM L57D04a, 1957.

11. Seiff, Alvin, Sommer, Simon C., and Canning, Thomas N.: Some Experiments at High Supersonic Speeds on the Aerodynamic and Boundary-Layer Transition Characteristics of High-Drag Bodies of Revolution. NACA RM A56I05, 1957.

12. Seiff, Alvin: A Review of Recent Information on Boundary-Layer Transition at Supersonic Speeds. NACA RM A55L21, 1956.

13. Canning, Thomas N., and Sommer, Simon C.: Investigation of Boundary-Layer Transition on Flat-Faced Bodies of Revolution at High Supersonic Speeds. NACA RM A57C25, 1957.

14. Moorman, Emily P.: Free-Flight Rocket Materiel Characteristics. Rep. No. A-10-a, Res. and Dev. Div., Ord. Missile Labs., Redstone Arsenal, Huntsville (Ala.). (Revised June 1, 1956.) (Proj. TU2-7C.)

15. Hilsenrath, Joseph, et al.: Tables of Thermal Properties of Gases, NBS Circular 564, Nov. 1, 1955.

16. Keenan, Joseph H., and Kaye, Joseph: Gas Tables. John Wiley & Sons, Inc., 1948.

17. Wang, Chi-Teh, and DeSanto, Daniel F.: Differentiation of Experimental Data by Means of Higher Order Finite-Difference Formulas. Jour. Aero. Sci., vol. 20, no. 11, Nov. 1953, pp. 792-793.

18. Anon.: Nickel and Its Alloys. Circular 485, NBS, Mar. 22, 1950.

4522

[redacted]

19. Oliver, Robert E.: An Experimental Investigation of Flow over Simple Blunt Bodies at a Nominal Mach Number of 5.8. Memo. No. 26, GALCIT, June 1, 1955. (Contract No. DA-04-495-Ord-19.)

20. Crawford, Davis H., and McCauley, William D.: Investigation of the Laminar Aerodynamic Heat-Transfer Characteristics of a Hemisphere-Cylinder in the Langley 11-Inch Hypersonic Tunnel at a Mach Number of 6.8. NACA TN 3706, 1956.

21. Hill, P. R.: A Method of Computing the Transient Temperature of Thick Walls From Arbitrary Variation of Adiabatic Wall Temperature and Heat-Transfer Coefficient. NACA TN 4105, 1957.

22. van Driest, E. R.: The Problem of Aerodynamic Heating. Aero. Eng. Rev., vol. 15, no. 10, Oct. 1956, pp. 26-41.

23. Cohen, Clarence B., and Reshotko, Eli: The Compressible Laminar Boundary Layer with Heat Transfer and Arbitrary Pressure Gradient. NACA Rep. 1294, 1955. (Supersedes NACA TN 3326.)

24. Dunn, D. W., and Lin, C. C.: On the Stability of the Laminar Boundary Layer in a Compressible Fluid. Jour. Aero. Sci., vol. 22, no. 7, July 1955, pp. 455-477.

25. Lees, Lester: Note on the Stabilizing Effect of Centrifugal Forces on the Laminar Boundary Layer over Convex Surfaces. Rep. No. GM-TR-118, Guided Missile Res. Div., The Ramo-Wooldridge Corp., Dec. 14, 1956. (Contract No. AF 18(600)-1190.)

TABLE I. - PHYSICAL DATA OF SINGLE-STAGE TEST BODY

Gross weight at launching, lb	409.0
Nozzle and motor, lb	82.4
Propellant, lb	262.5
Liner, lb	2.6
Nose skin, lb	12.0
Telemeter package including antenna, lb	19.5
Fin section, lb	30.0
Center of gravity at launching,[a] in.	67.0
Body diameter, in.	9.0
Hemisphere-cylinder skin material	Nickel
Surface finish of instrumented hemisphere-cylinder, microin. rms	~ 3 to 5

[a]From nose tip.

[redacted]

TABLE II. - THERMOCOUPLE AND PRESSURE TAP DATA

(a) Thermocouple

Station (see fig. 2)	Angle on a sphere between stagnation point and a given station, α, deg	Surface distance from stagnation point, x, ft	Ratio of surface distance from stagnation point to semi-hemispherical arc length, x/b or $4x/\pi D$	Skin thickness at thermocouple station, in.
A	0	0	0	0.0597
B	11.5 Outside	.075	.127	.0510
C	11.5 Inside	-----	-----	.0512
D	22.75	.149	.253	.0540
E	34.0	.223	.379	.0591
F	45.0	.295	.501	.0602
G	46.5 Inside	.305	.518	.0594
H	57.0	.374	.635	.0662
I	69.0	.452	.767	.0720
J	81.0	.531	.902	.0679
[a]K	----	.712	1.209	.0519
[a]L	----	1.609	2.730	.0560

(b) Pressure tap

Station	Angle on a sphere between stagnation point and a given station, α, deg	Surface distance from stagnation point, x, ft	Ratio of surface distance from stagnation point to semi-hemispherical arc length, x/b or $4x/\pi D$	Pressure orifice diameter, in.
M	11.25	0.074	0.125	0.067
N	45.0	.295	.501	.067
[b]Q	69.0	.452	.767	.067
P	-----	1.607	2.730	.067

[a]Station on cylinder.

[b]Data not used since transducer apparently stuck.

[redacted]

TABLE III. - SPECIFICATIONS AND RATED PERFORMANCE OF T-64 ROCKET ENGINE AT SEA LEVEL

[Data from ref. 15.]

Specifications	
Outside diameter, in.	9.0
Total length, in.	100.57
Total weight (unburned), lb	356.0
Total weight (burned), lb	81.0
Performance	
Temperature of rocket propellant, ^{o}F	70.0
Average thrust, lb	33,900.0
Total impulse, lb-sec	51,600.0
Specific impulse, lb-sec/lb	218.0
Burning time, sec	1.52

TABLE IV. - TRANSITION PARAMETERS

M_1	$Re_{1,D}$	$\tilde{Re}_{tr}$	$\tilde{Re}$ at sonic point	$Re_{tr,l}$	Re_l at sonic point	$Re_{\theta,tr}$ (a)	Re_θ at sonic point (a)	$\left(\frac{k}{\theta}\right)_{stagnation}$ region
2.07	6.6×10^6	$<0.048\times10^6$	0.72×10^6	$<0.20\times10^6$	2.22×10^6	<144	565	0.0084
2.70	8.7	<.058	.88	<.20	2.67	<160	620	.0088
3.36	11.0	<.067	.99	<.21	3.01	<172	661	.0088
4.01	13.4	<.074	1.06	<.25	3.30	<181	687	.0088
4.90	17.0	<.081	1.15	<.26	3.69	<189	712	.0090
5.48	19.5	<.084	1.20	<.26	3.89	<192	724	.0091

[a]Reynolds numbers based on momentum thickness calculated using method of ref. 8 agree well with the more exact method of ref. 19.

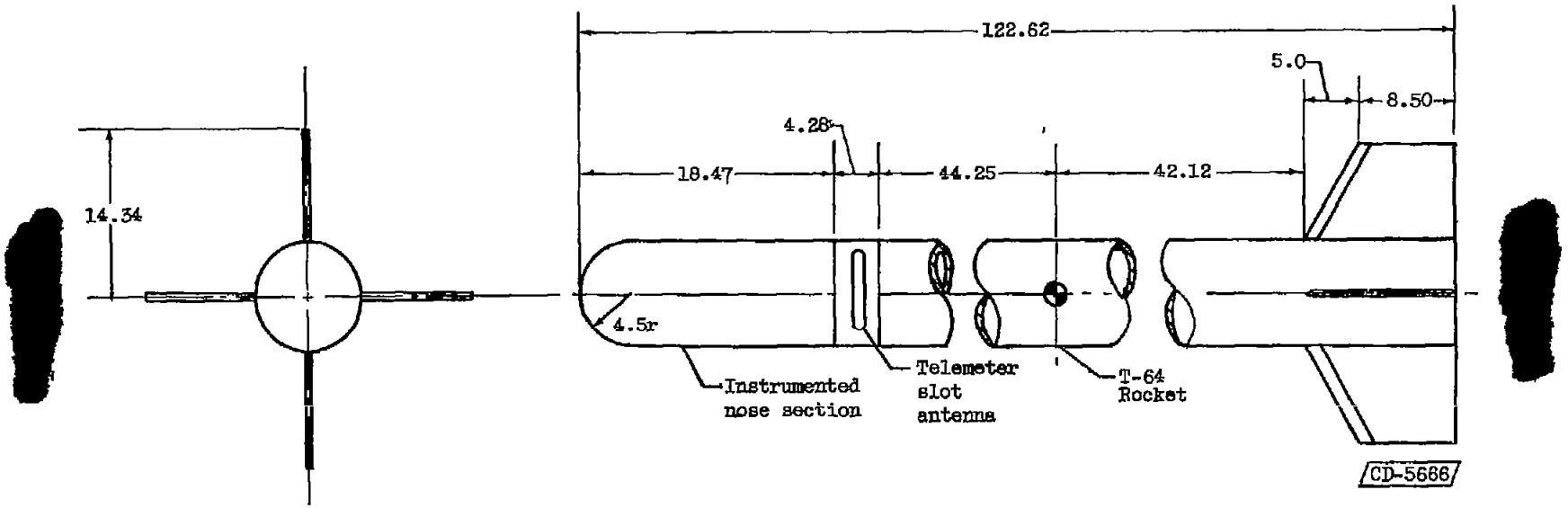

Figure 1. - Physical data of test body. (All dimensions in inches.)

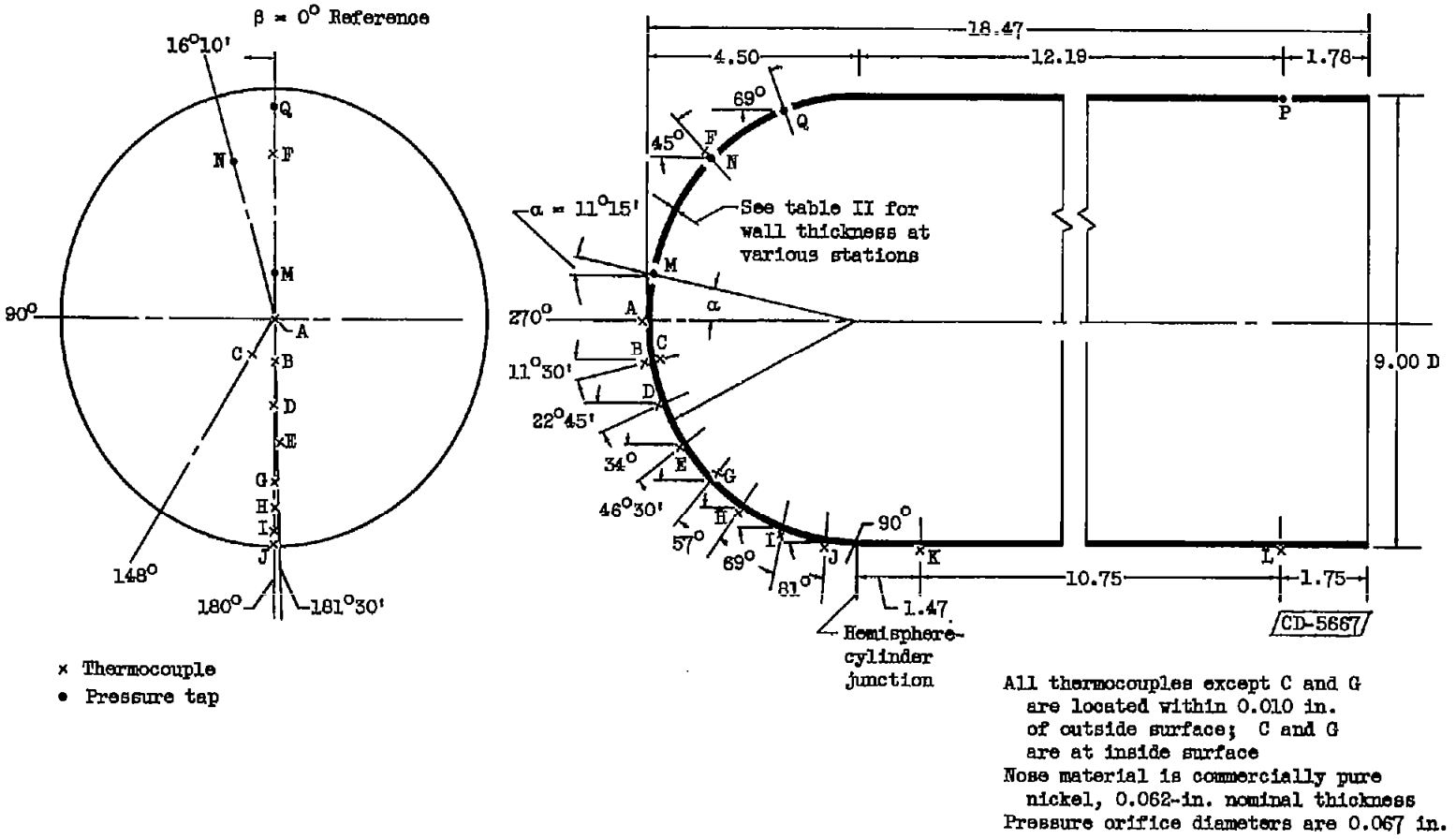

Figure 2. - Thermocouple and pressure tap locations. (All dimensions in inches.)

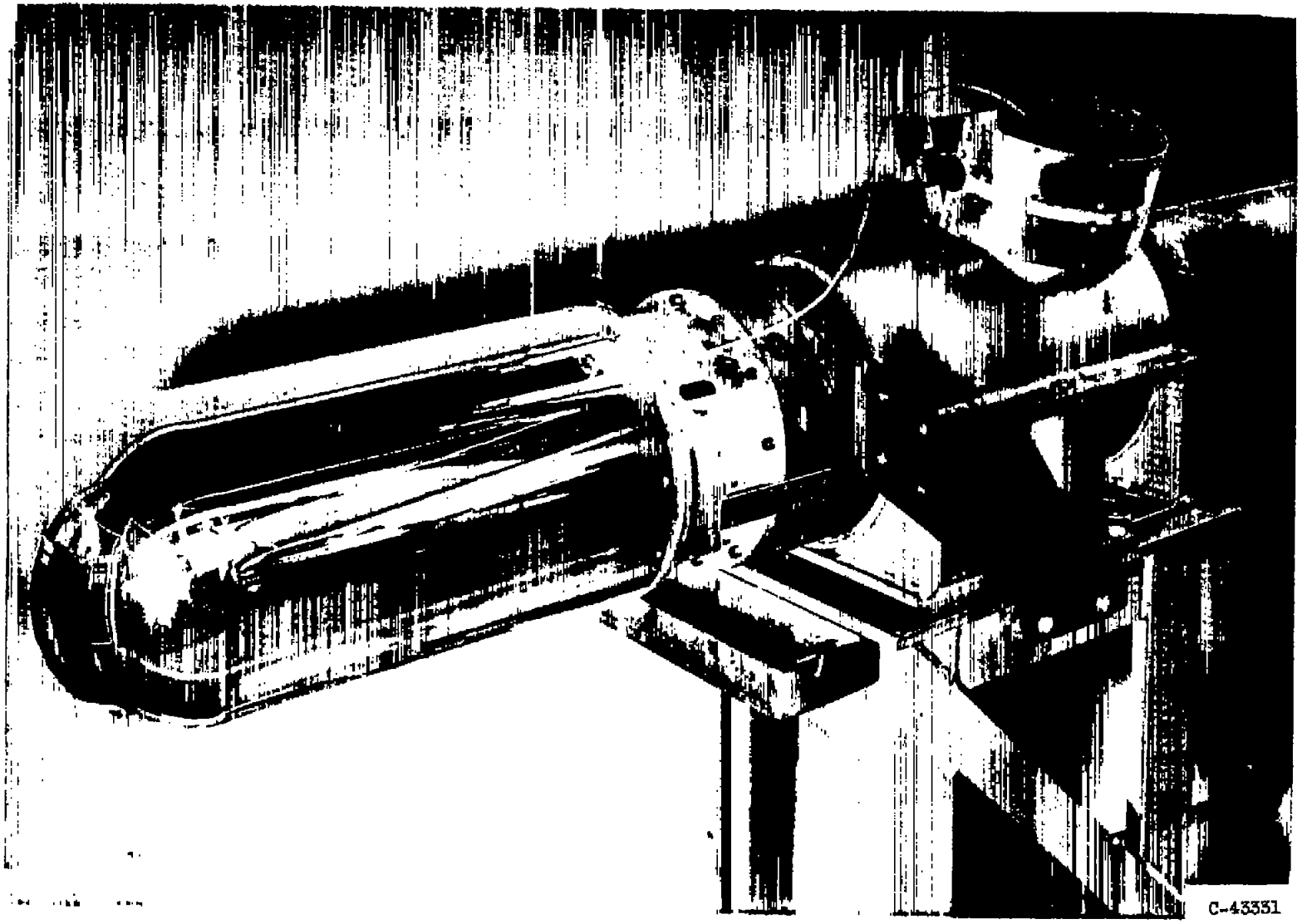

Figure 3. - Instrumented forebody.

C-43328

Figure 4. - Test vehicle.

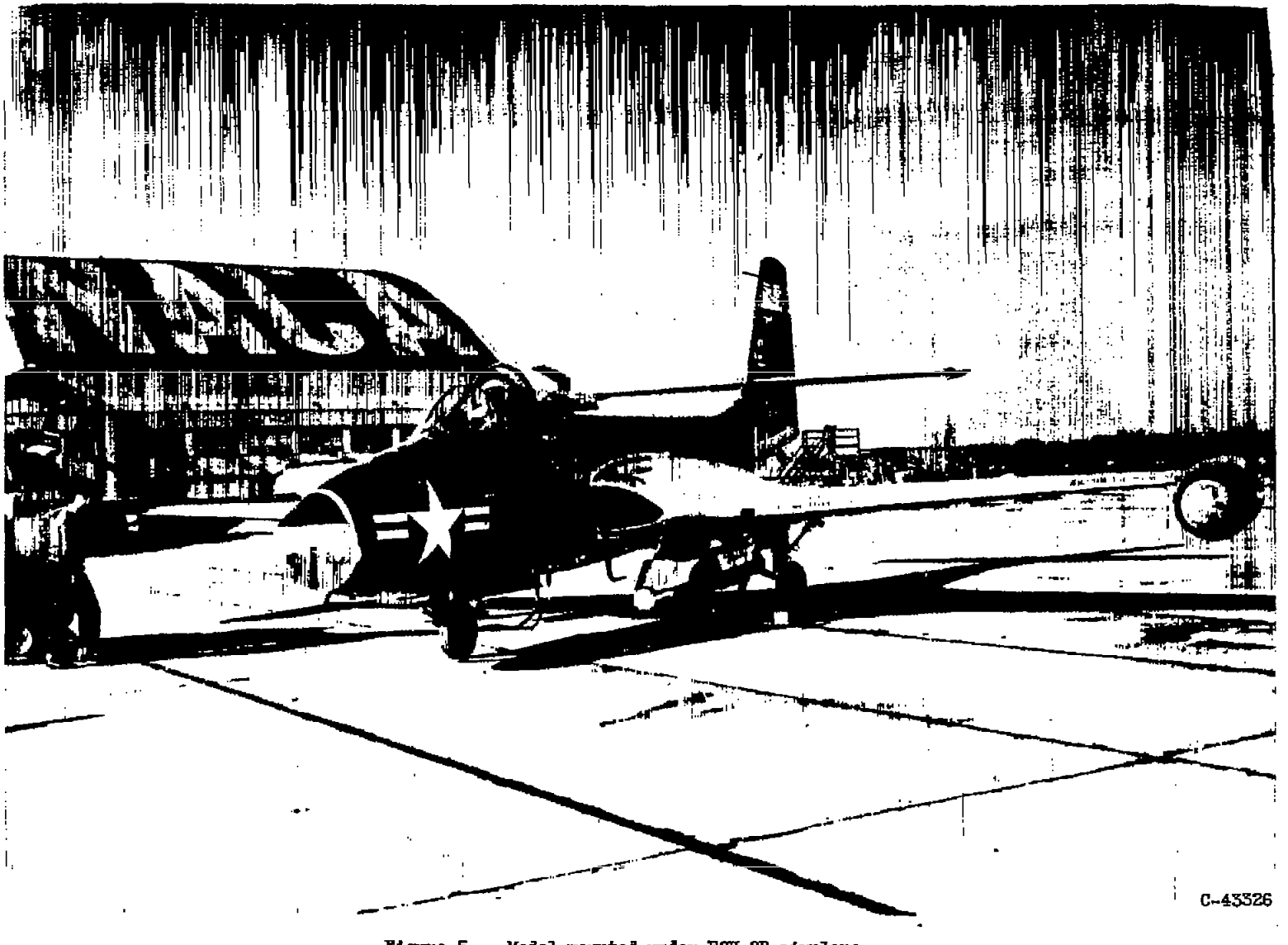

Figure 5. - Model mounted under F2H-2B airplane.

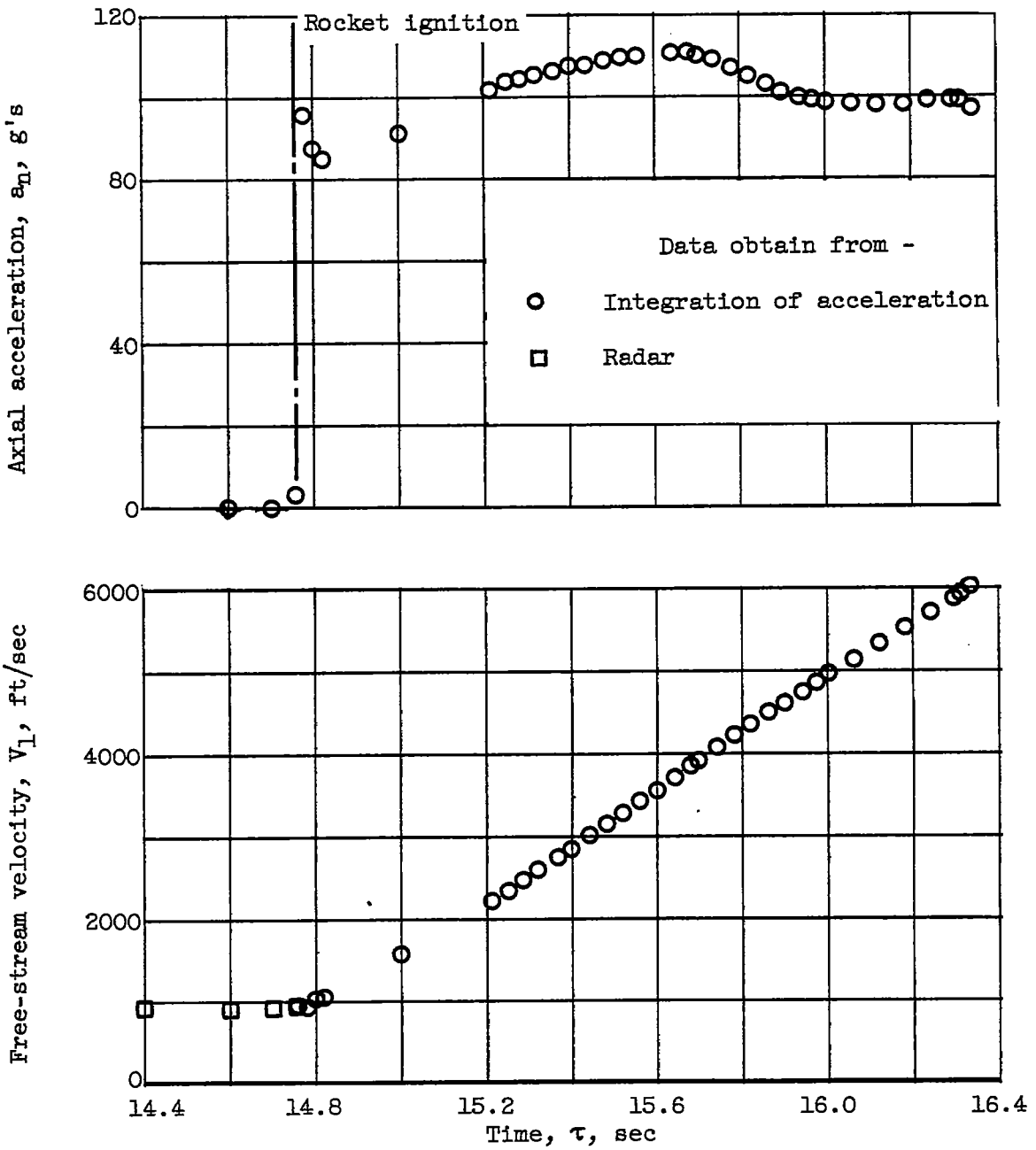

Figure 6. - Variation of axial acceleration and free-stream velocity with time.

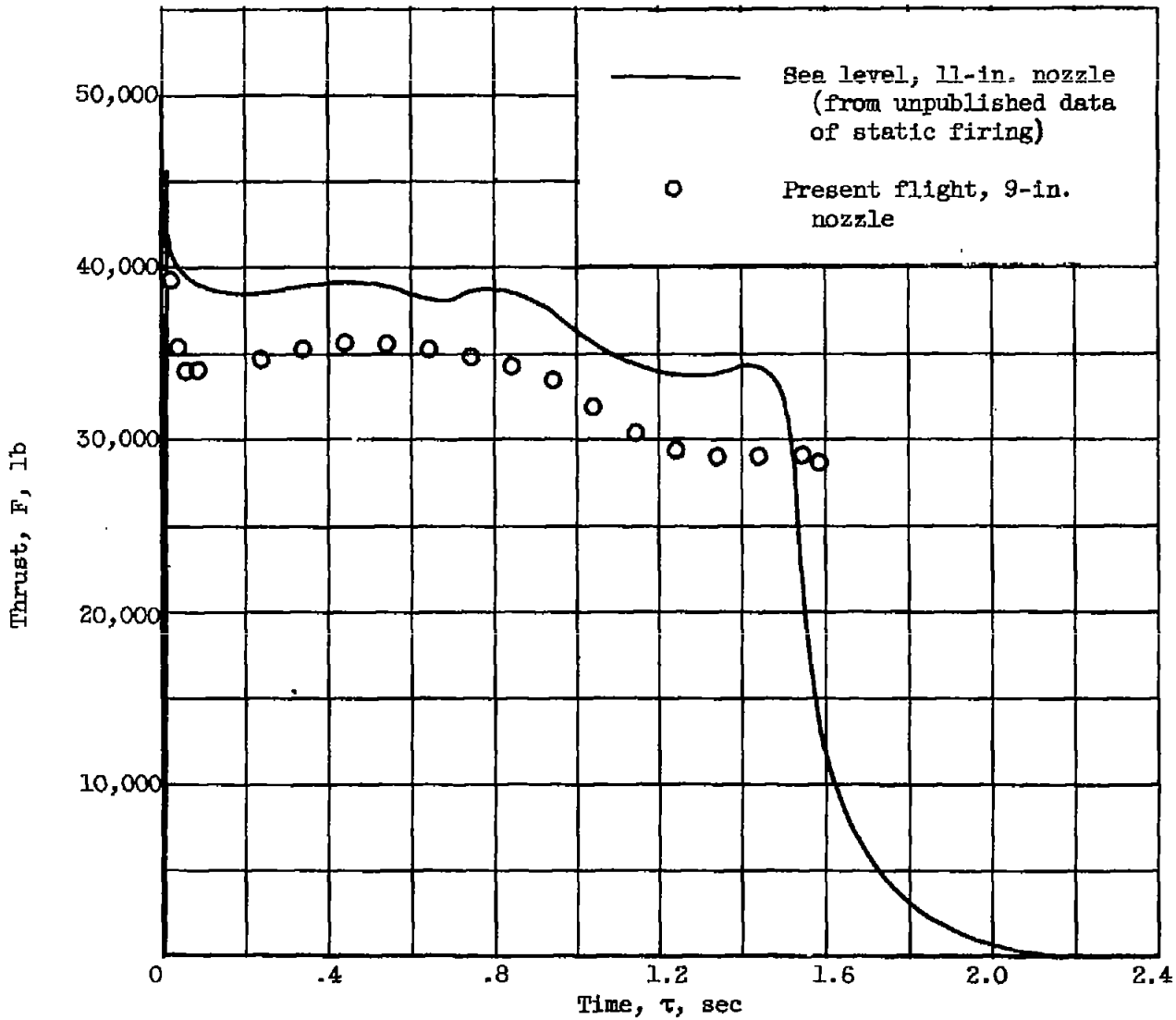

Figure 7. - Comparison of rocket thrust and time at sea level with flight.

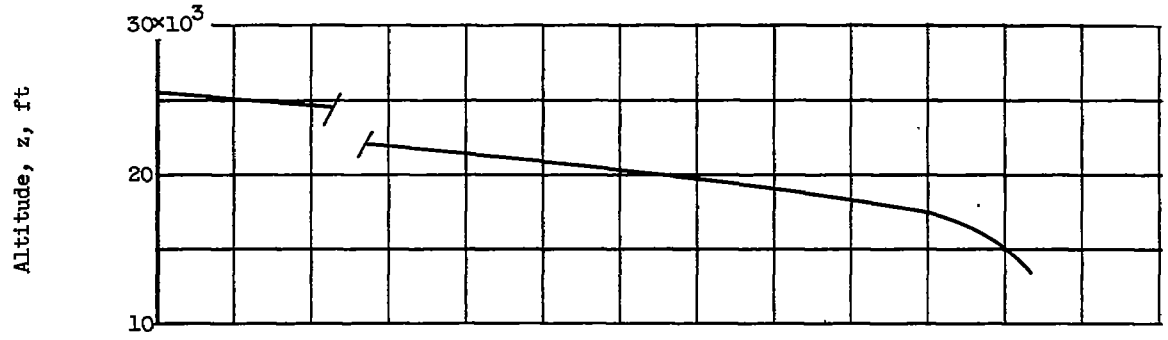

(a) Altitude.

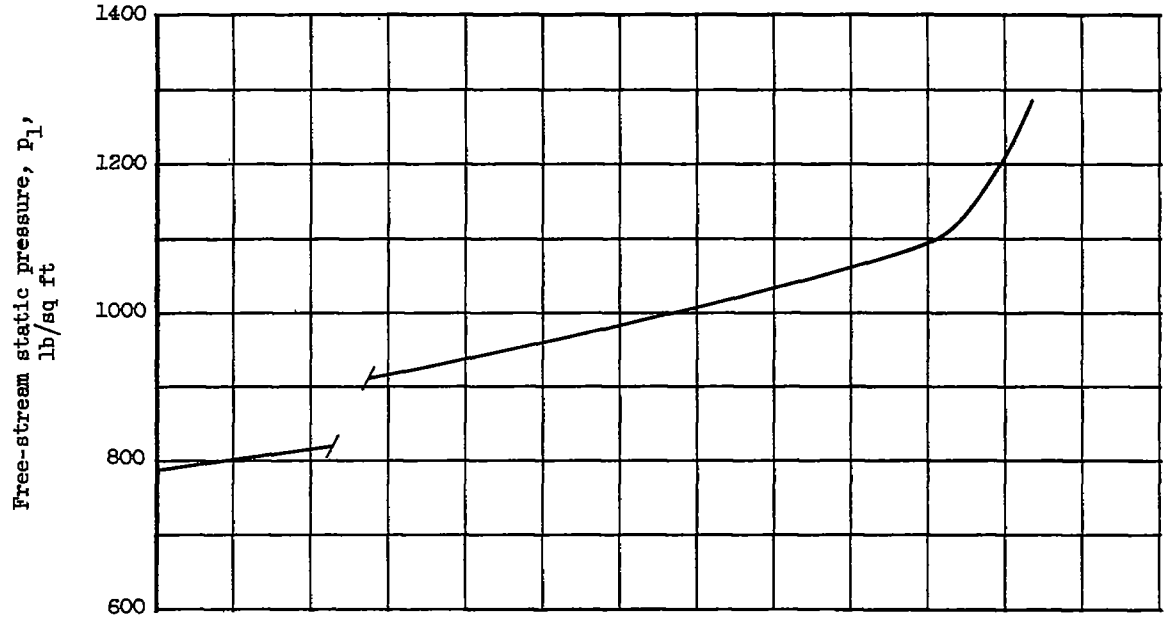

(b) Free-stream static pressure.

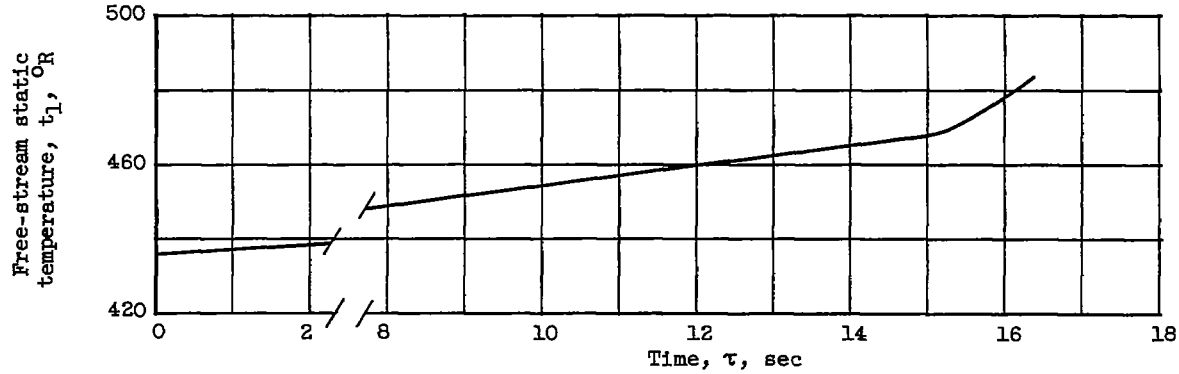

(c) Free-stream static temperature.

Figure 8. - Variation of free-stream conditions with time.

[redacted]

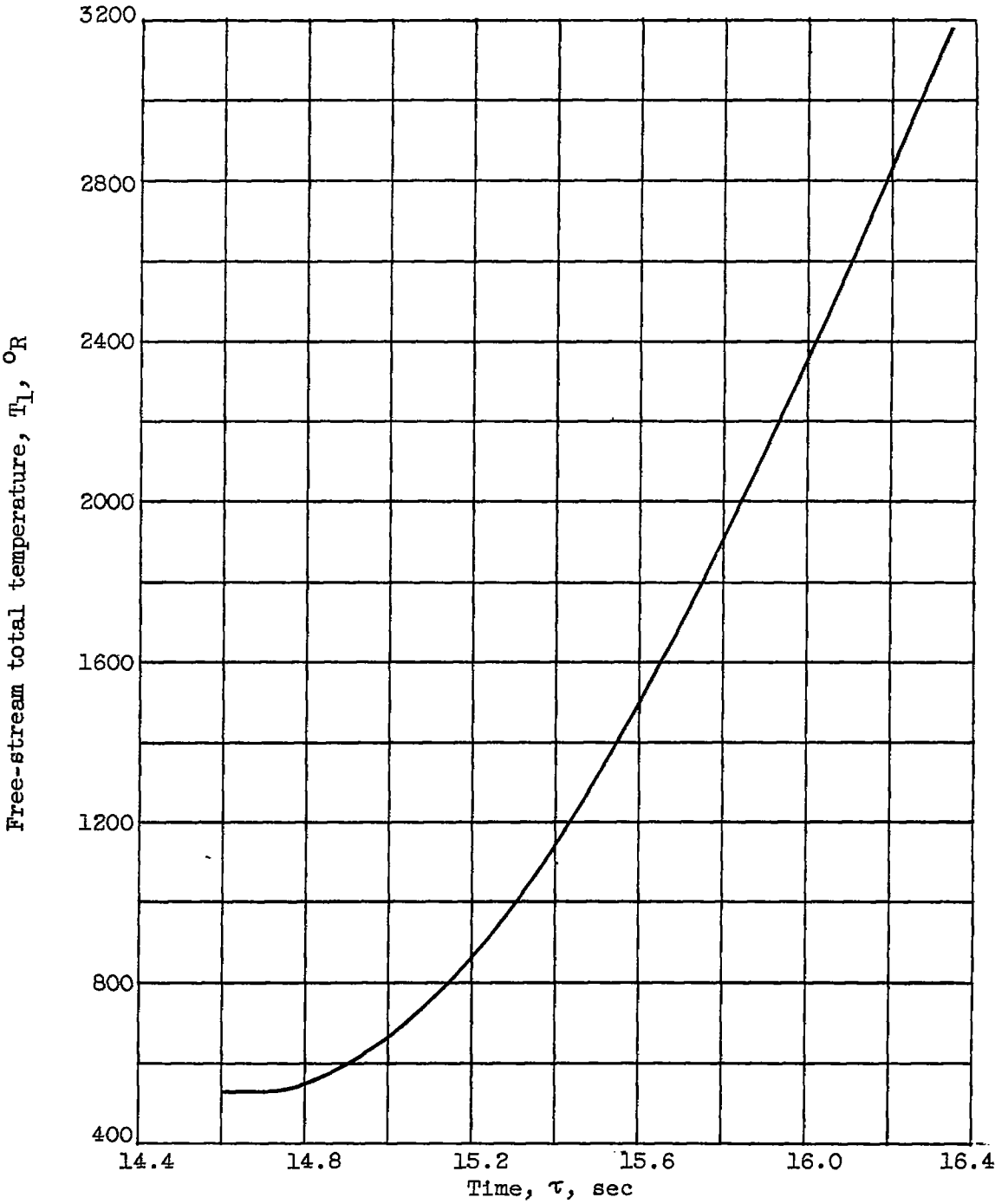

(d) Total temperature.

Figure 8. - Continued. Variation of free-stream conditions with time.

[redacted]

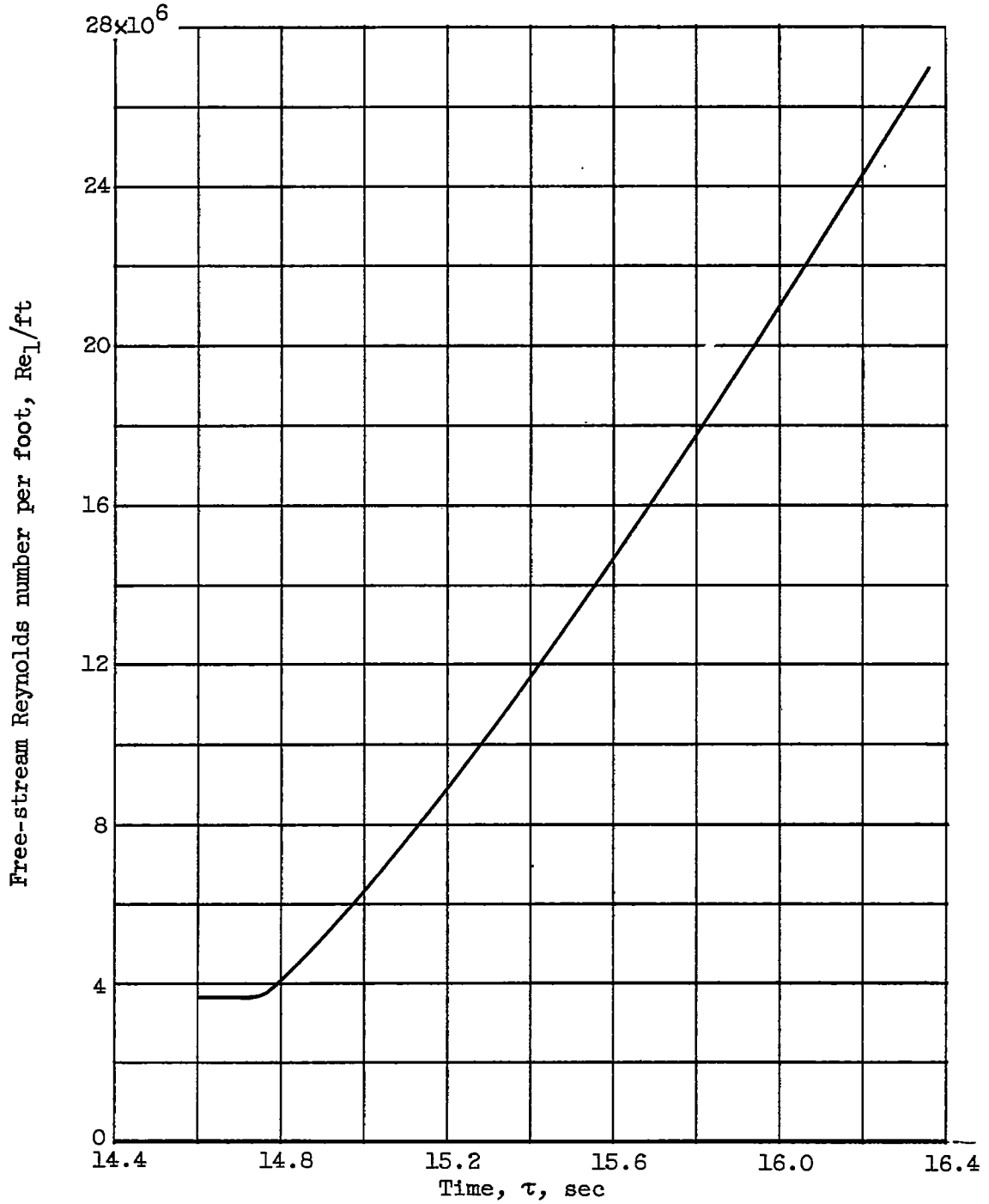

(e) Free-stream Reynolds number per foot.

Figure 8. - Continued. Variation of free-stream conditions with time.

[redacted]

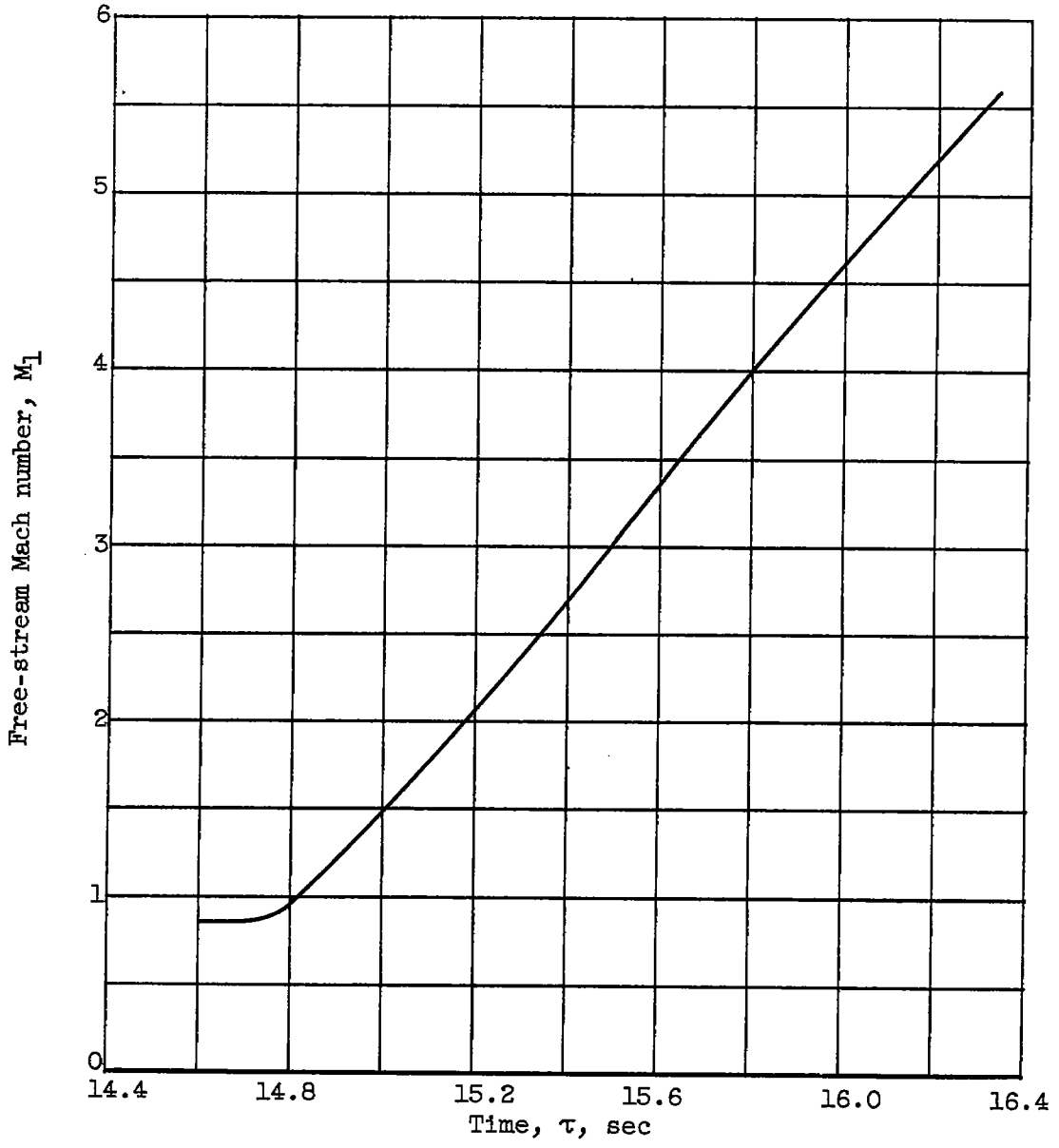

(f) Free-stream Mach number.

Figure 8. - Continued. Variation of free-stream conditions with time.

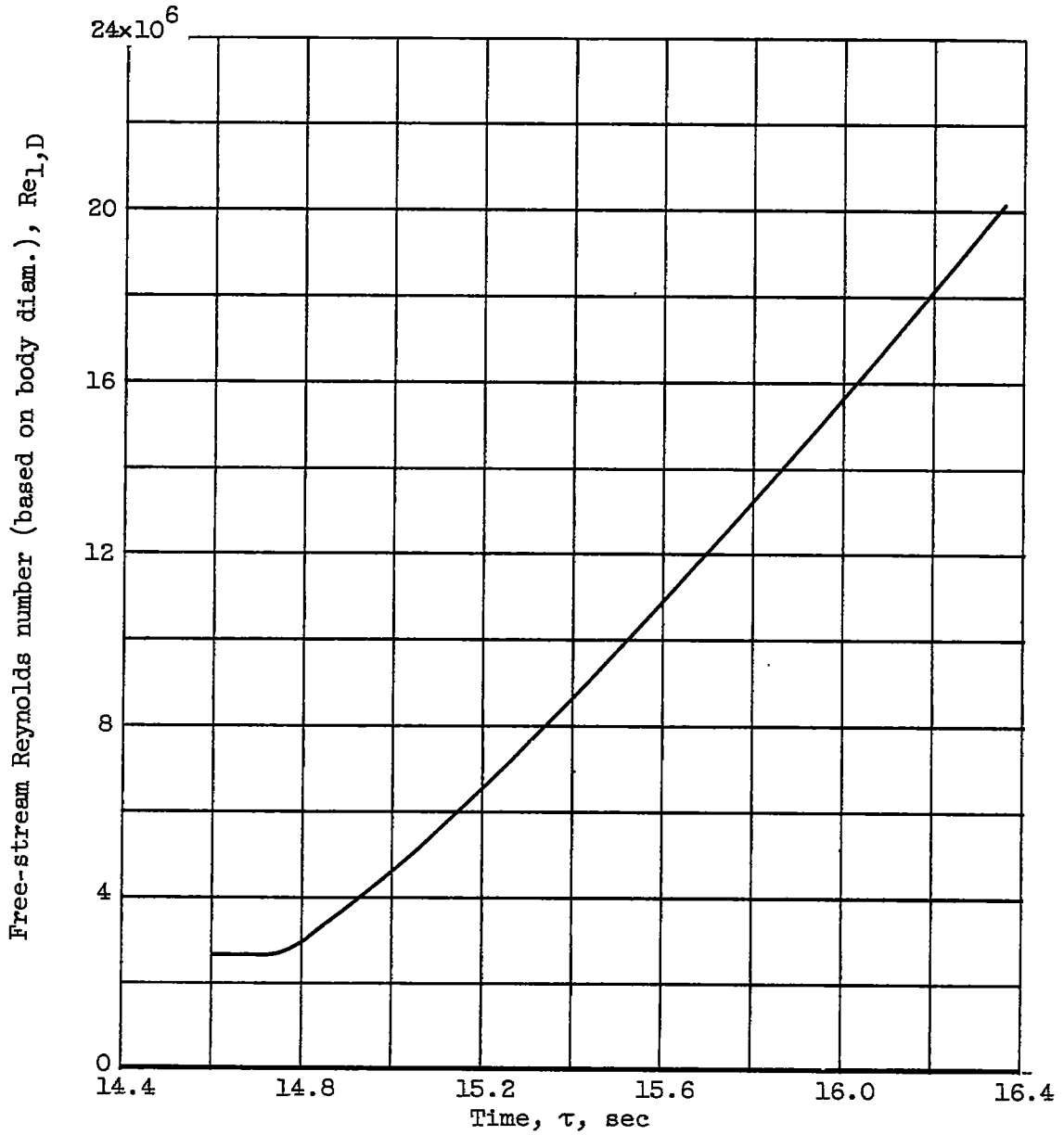

(g) Free-stream Reynolds number (based on body diam.).

Figure 8. - Concluded. Variation of free-stream conditions with time.

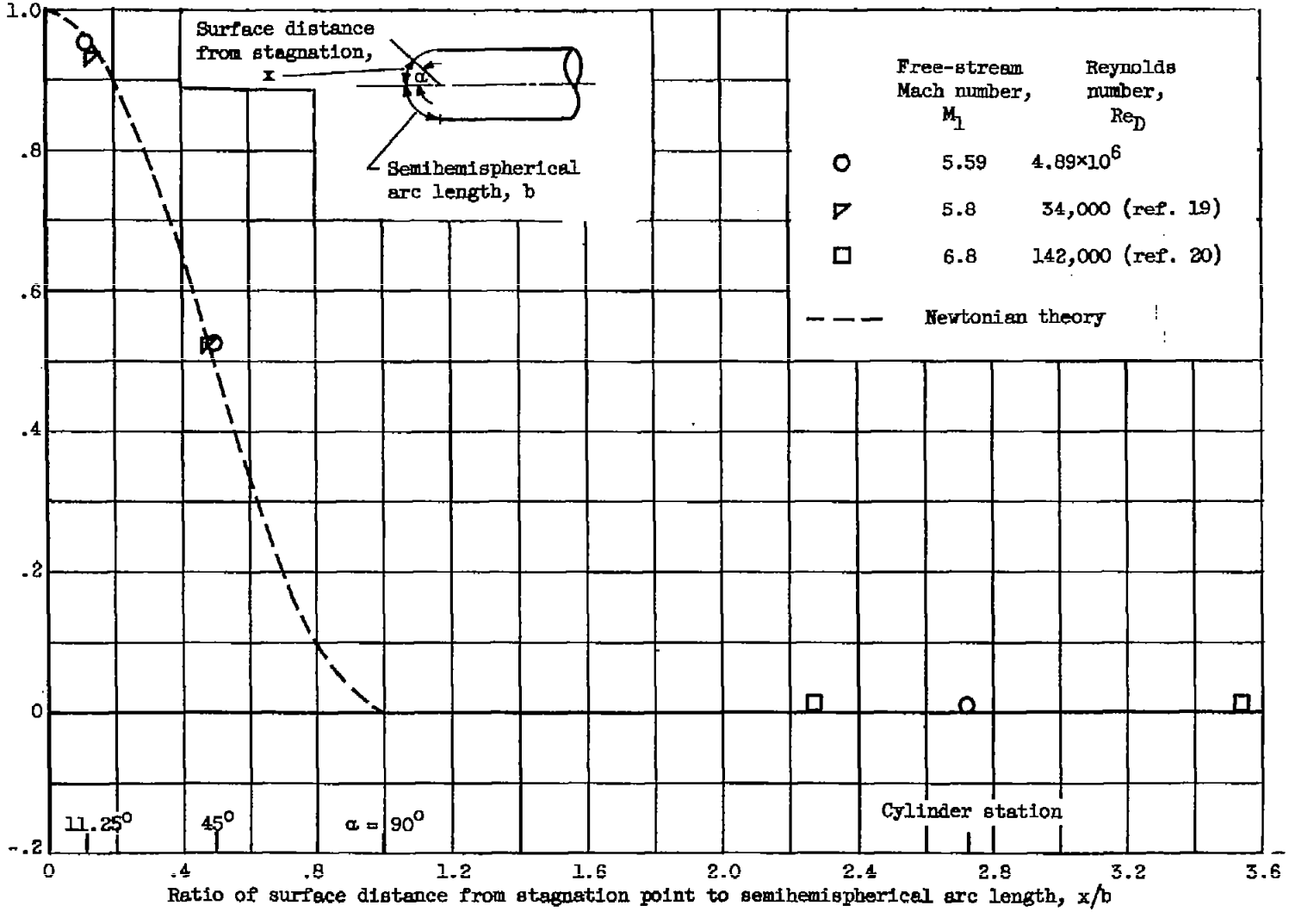

Figure 9. - Longitudinal pressure coefficient distribution.

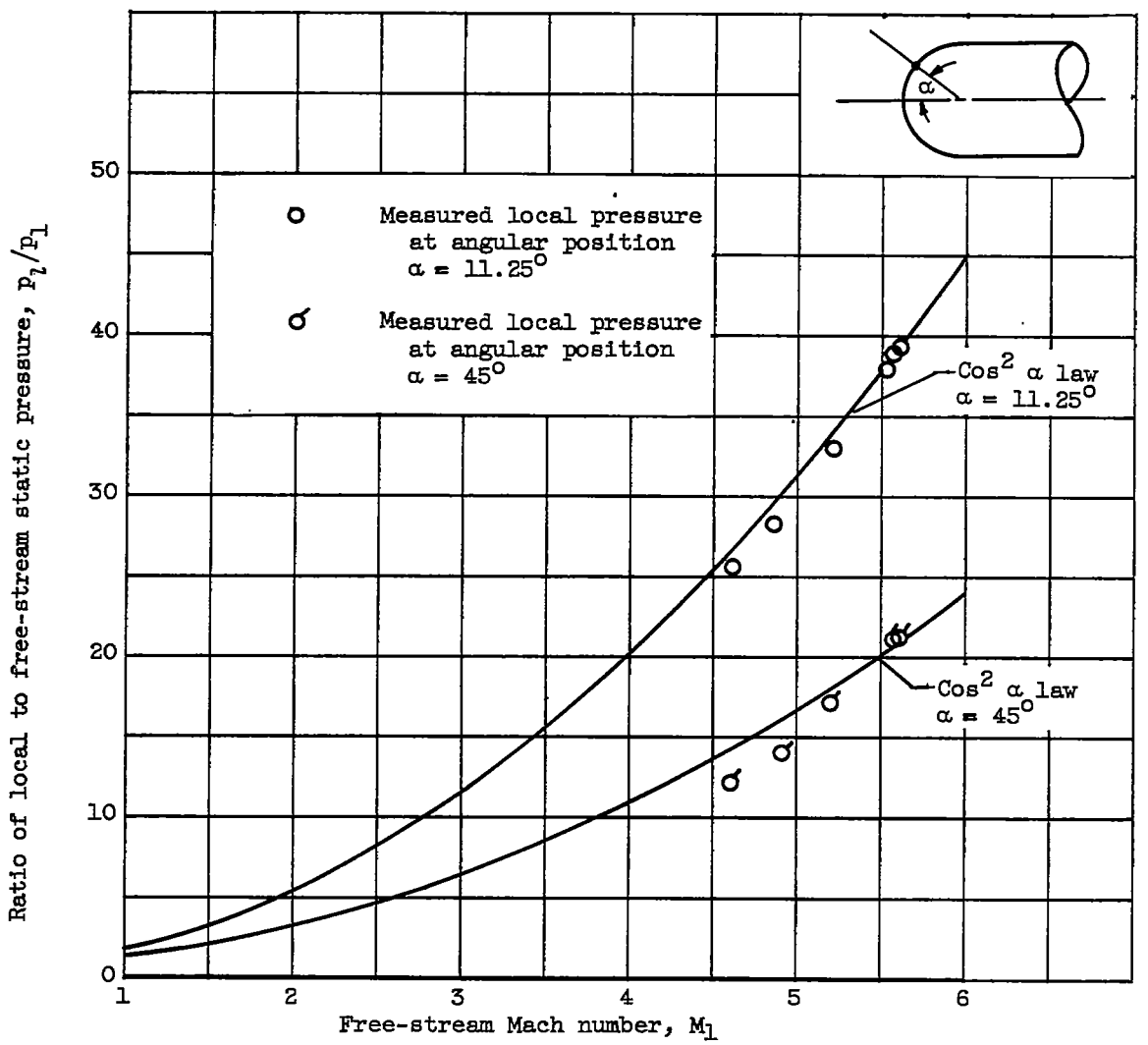

Figure 10. - Variation of local to free-stream static pressure at stations 11.25° and 45° with free-stream Mach number.

[redacted]

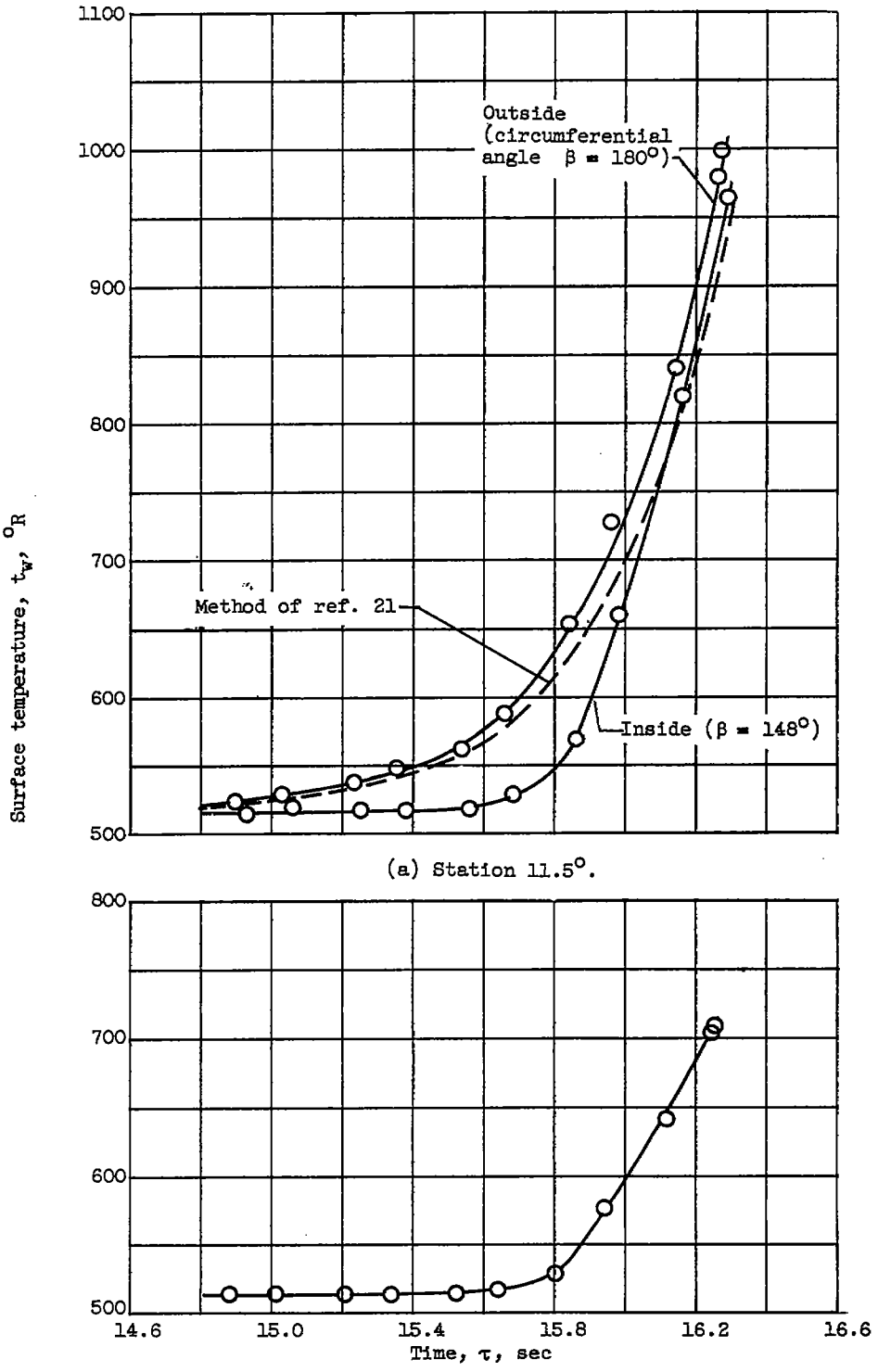

(a) Station 11.5°.

(b) Stagnation point.

Figure 11. - Variation of skin temperatures with time.

[redacted]

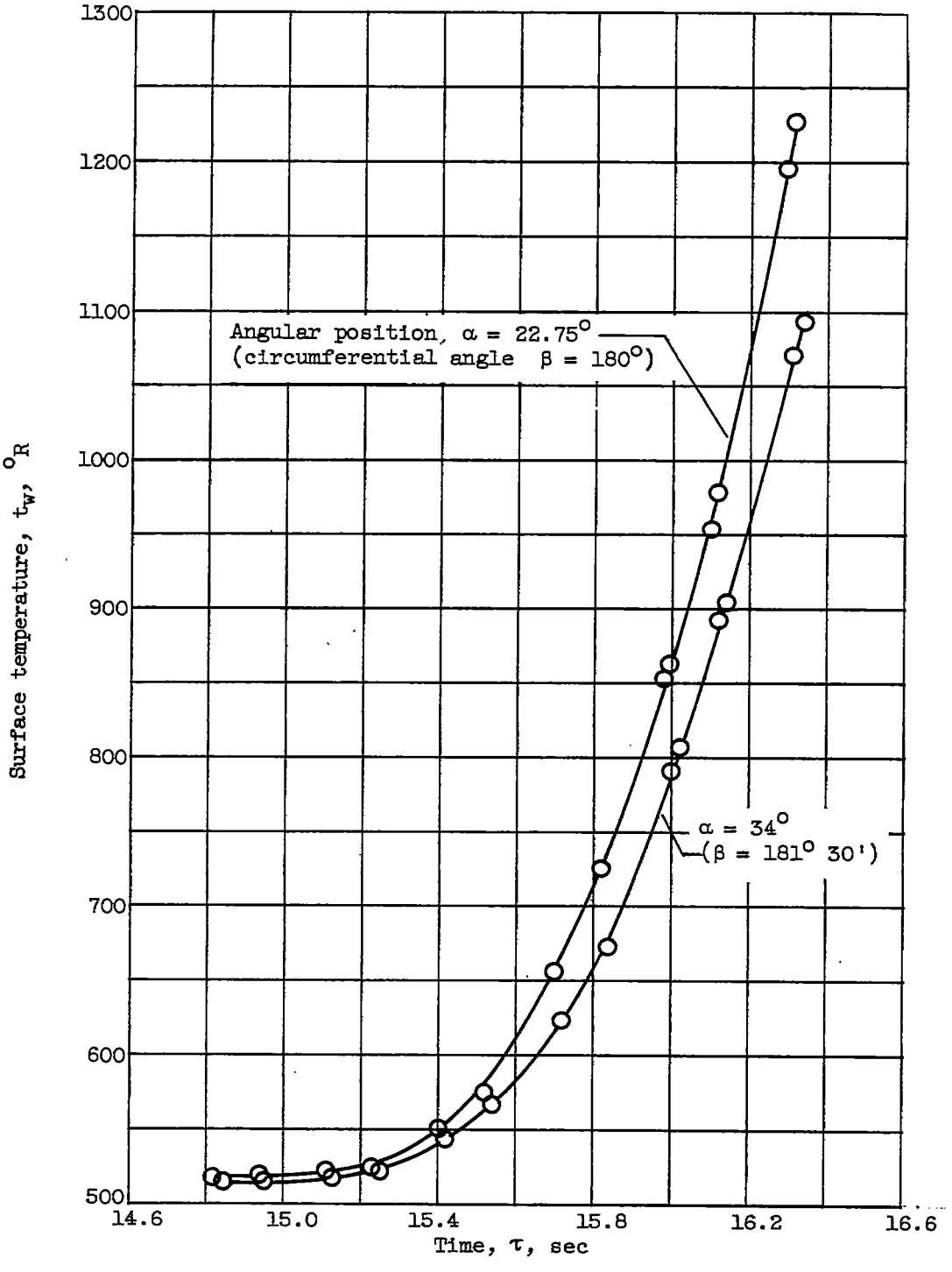

(c) Stations 22.75° and 34°.

Figure 11. - Continued. Variation of skin temperatures with time.

[redacted]

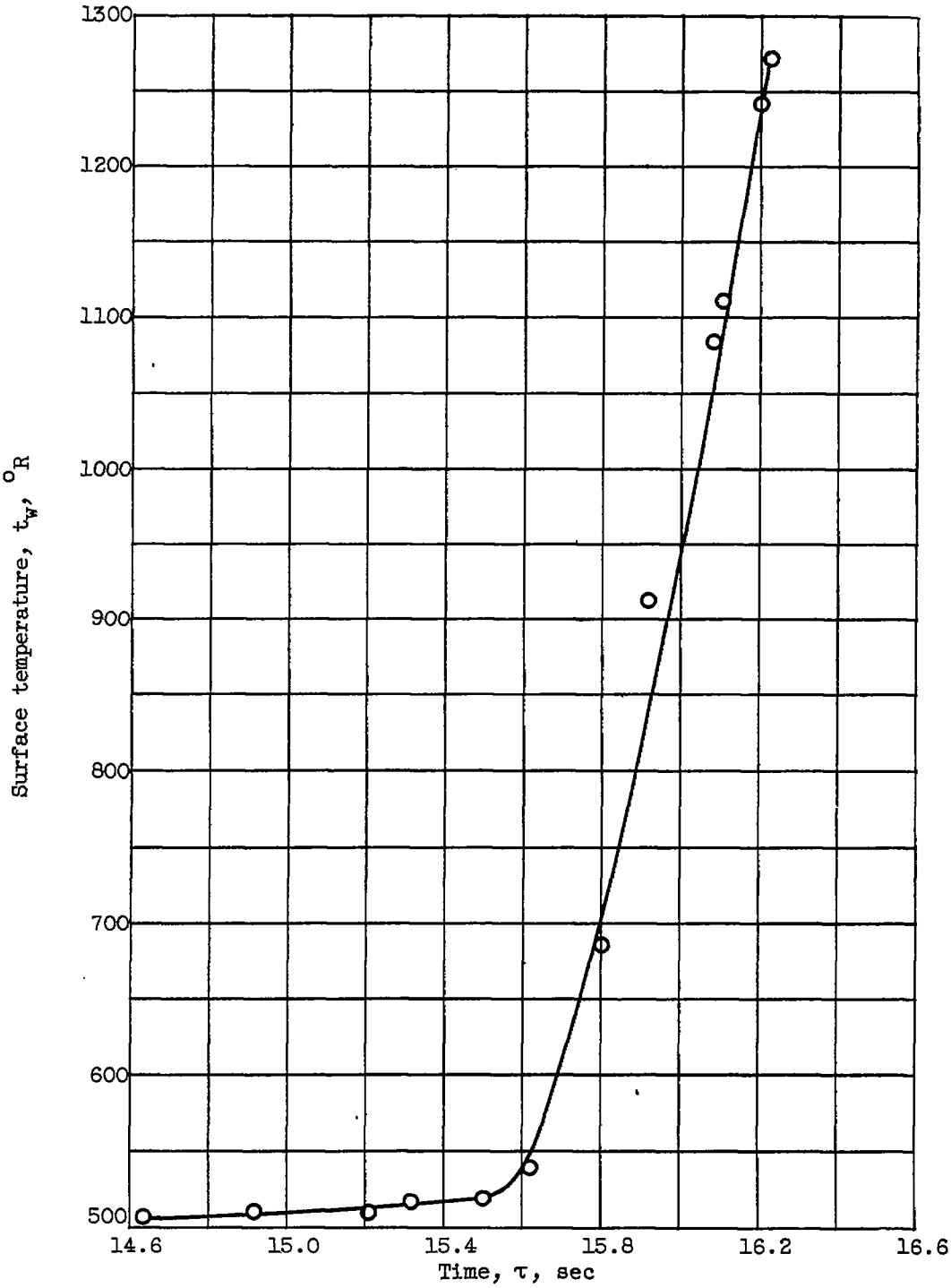

(d) Station 45°; circumferential angle, 0°.

Figure 11. - Continued. Variation of skin temperatures with time.

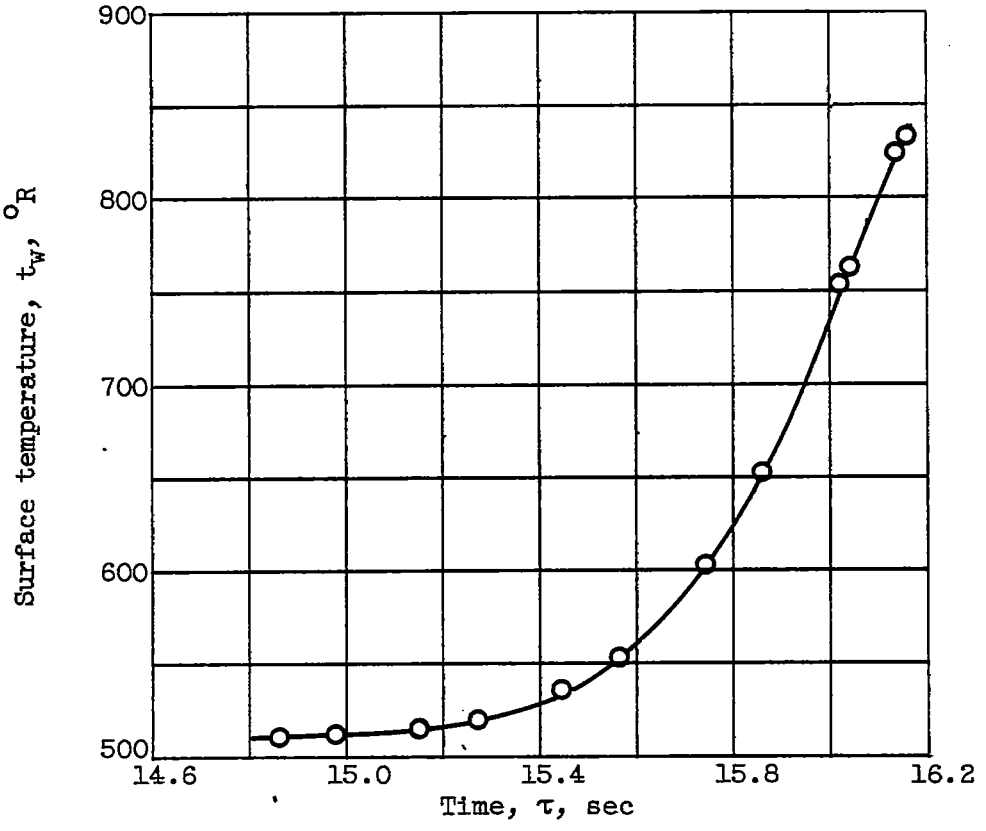

(e) Station 46.5° (inside); circumferential angle, 180°.

Figure 11. - Continued. Variation of skin temperatures with time.

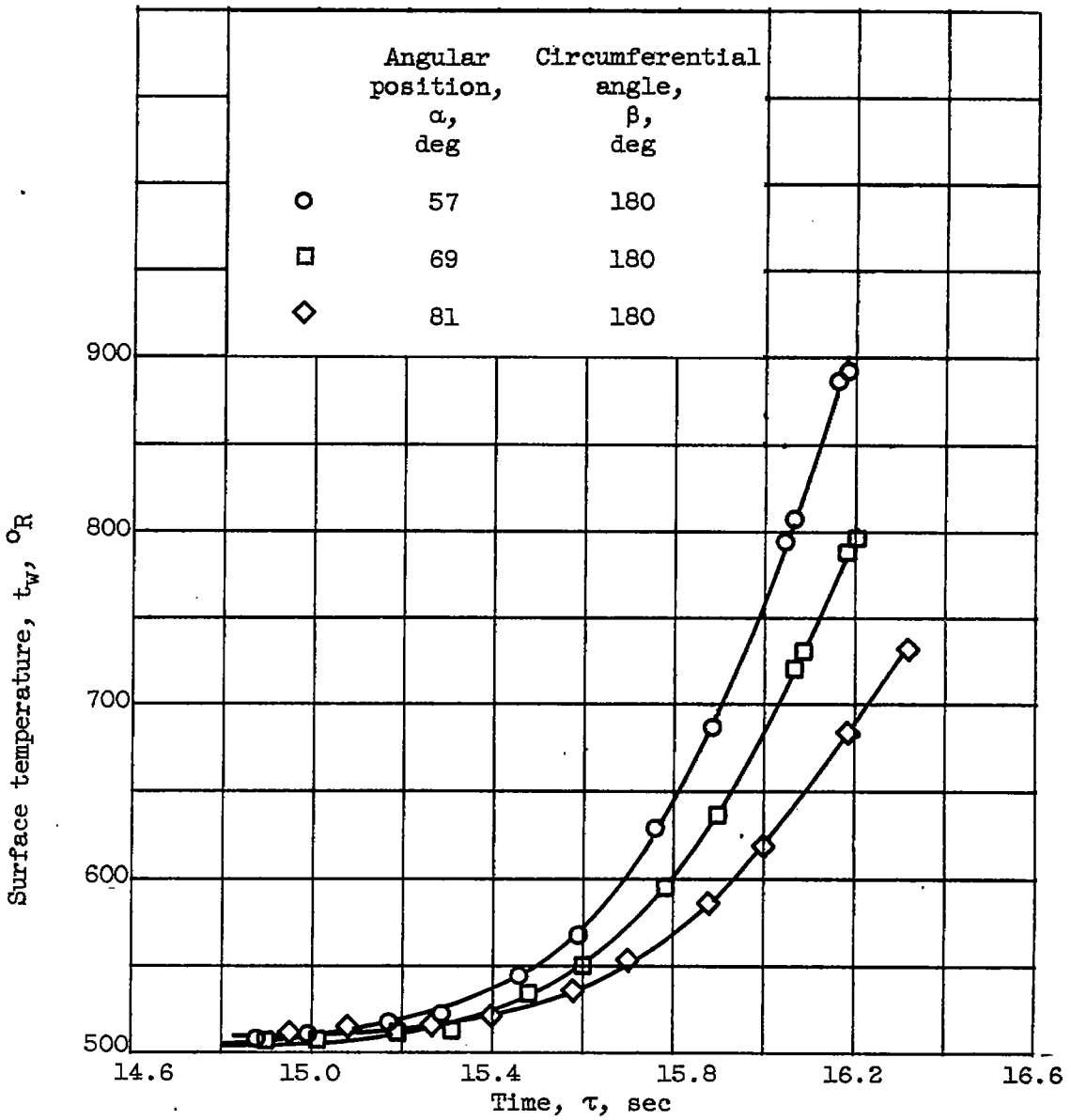

(f) Stations 57°, 69°, and 81°.

Figure 11. - Continued. Variation of skin temperatures with time.

[redacted]

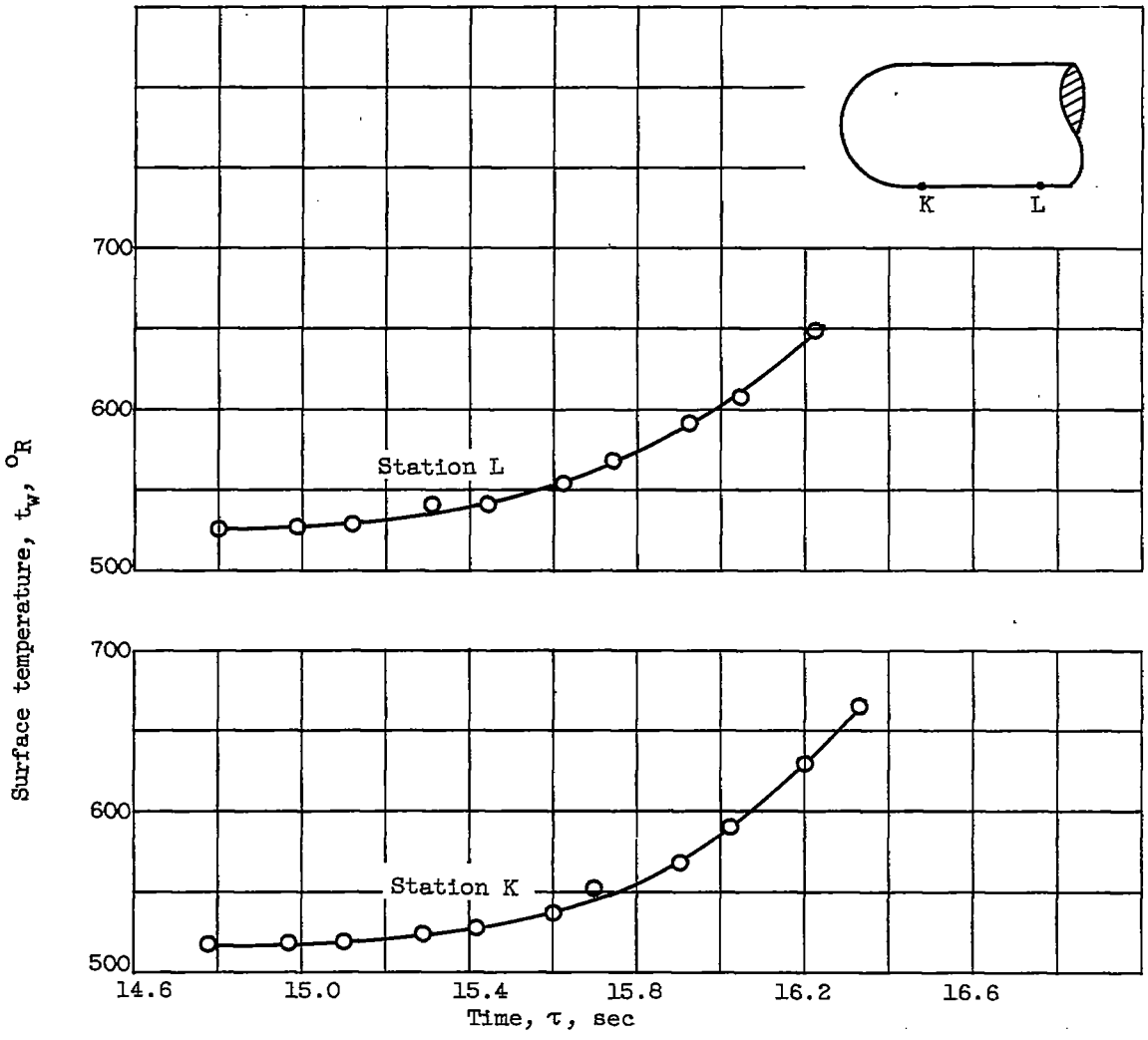

(g) Cylinder stations K and L; circumferential angle, 180°.

Figure 11. - Concluded. Variation of skin temperatures with time.

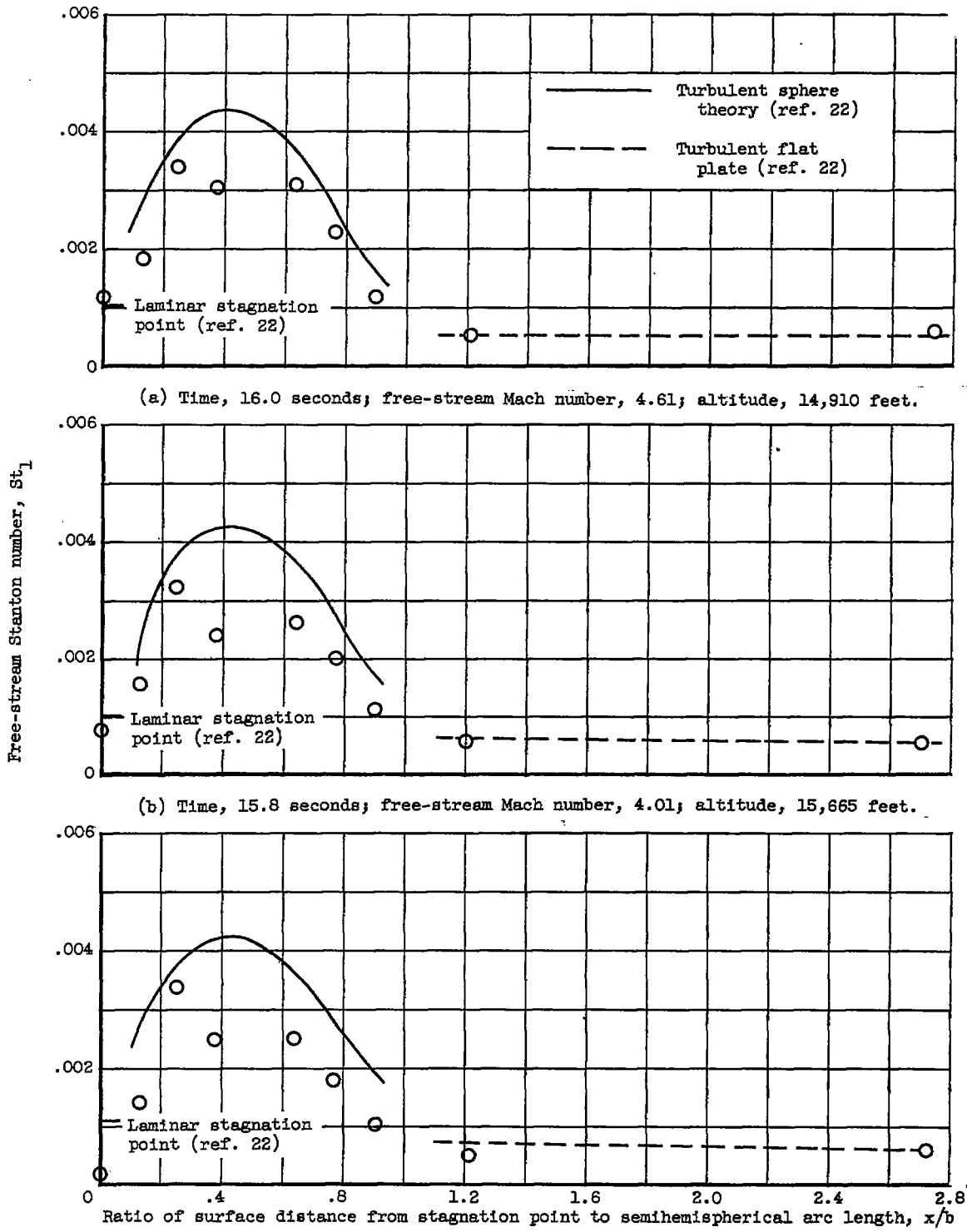

(a) Time, 16.0 seconds; free-stream Mach number, 4.61; altitude, 14,910 feet.

(b) Time, 15.8 seconds; free-stream Mach number, 4.01; altitude, 15,665 feet.

(c) Time, 15.6 seconds; free-stream Mach number, 3.36; altitude, 16,290 feet.

Figure 12. - Free-stream Stanton number at various times.

[redacted]

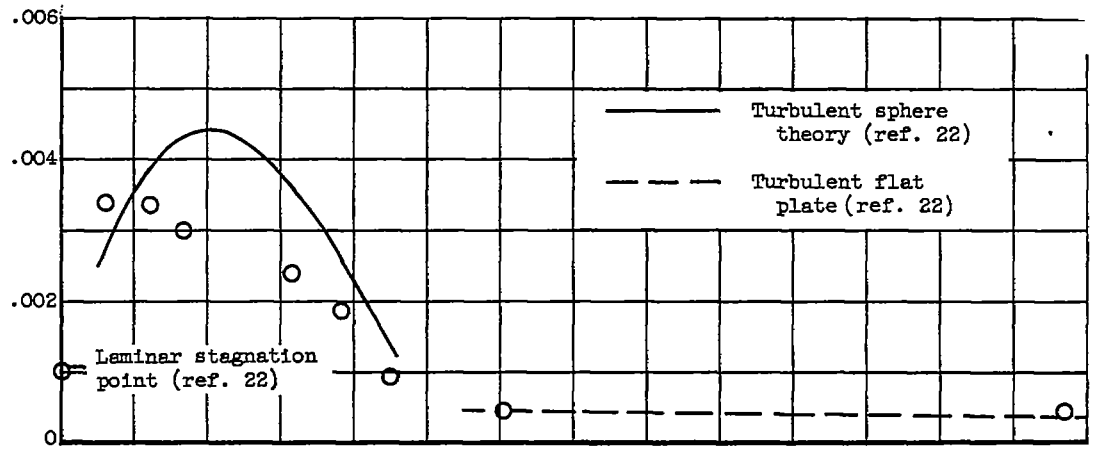

(d) Time, 16.3 seconds; free-stream Mach number, 5.48; altitude, 13,610 feet.

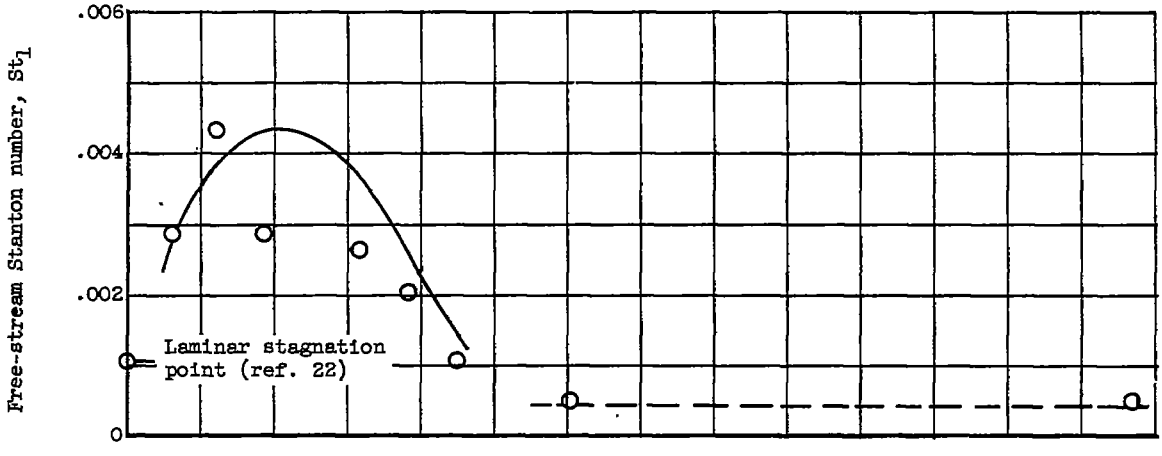

(e) Time, 16.2 seconds; free-stream Mach number, 5.19; altitude, 14,065 feet.

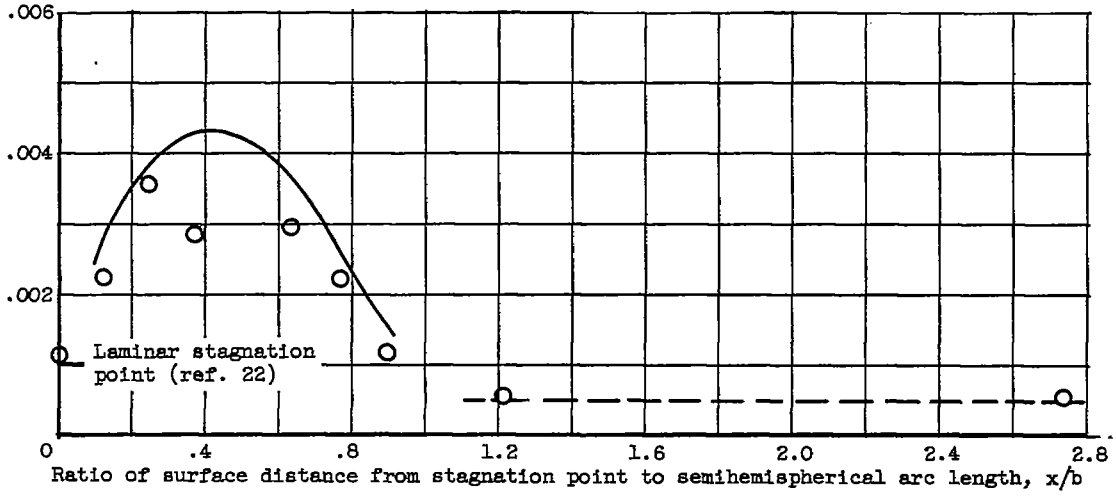

(f) Time, 16.1 seconds; free-stream Mach number, 4.90; altitude, 14,495 feet.

Figure 12. - Concluded. Free-stream Stanton number at various times.

[redacted]

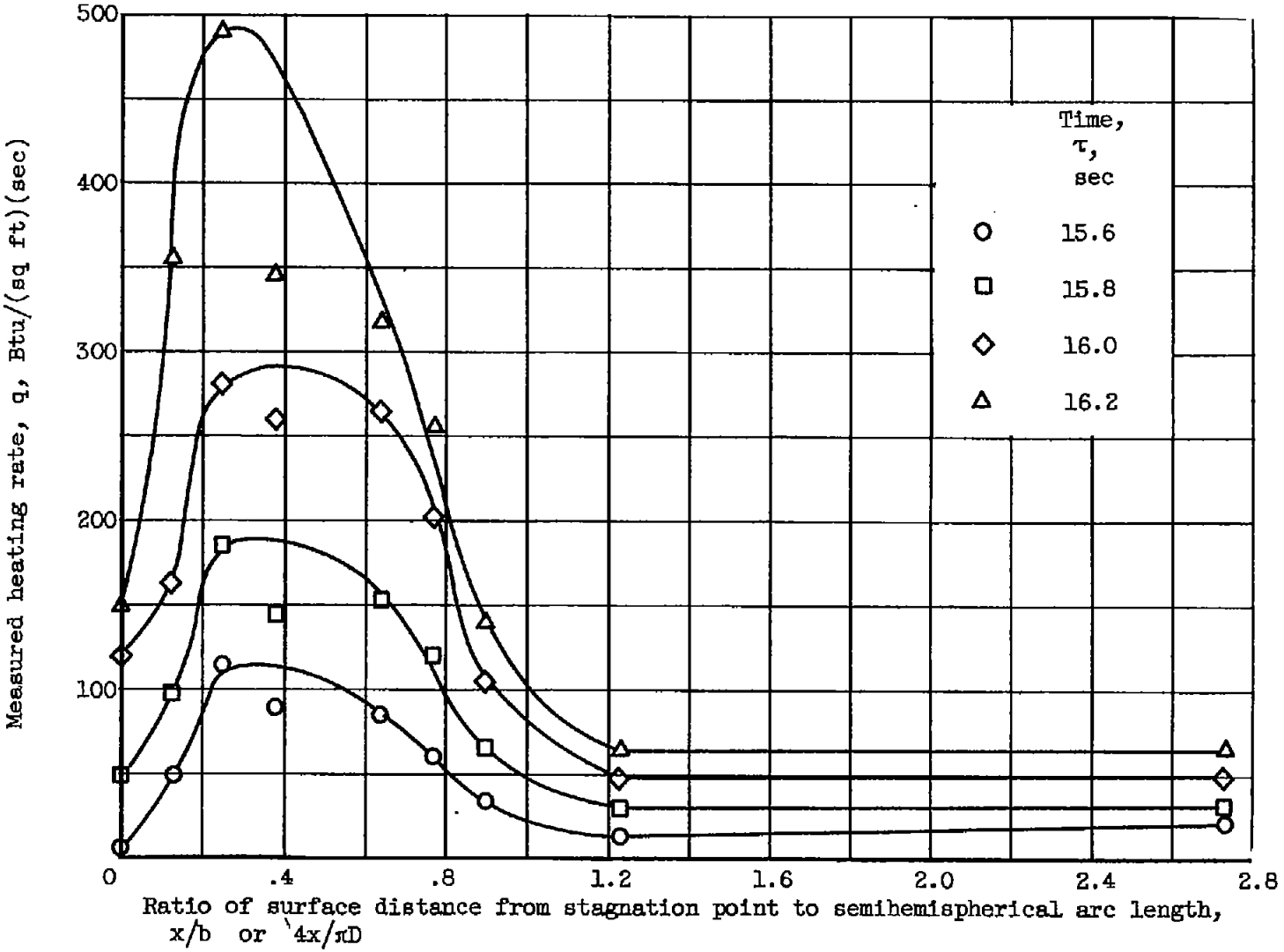

Figure 13. - Heating rate distributions on hemisphere-cylinder.

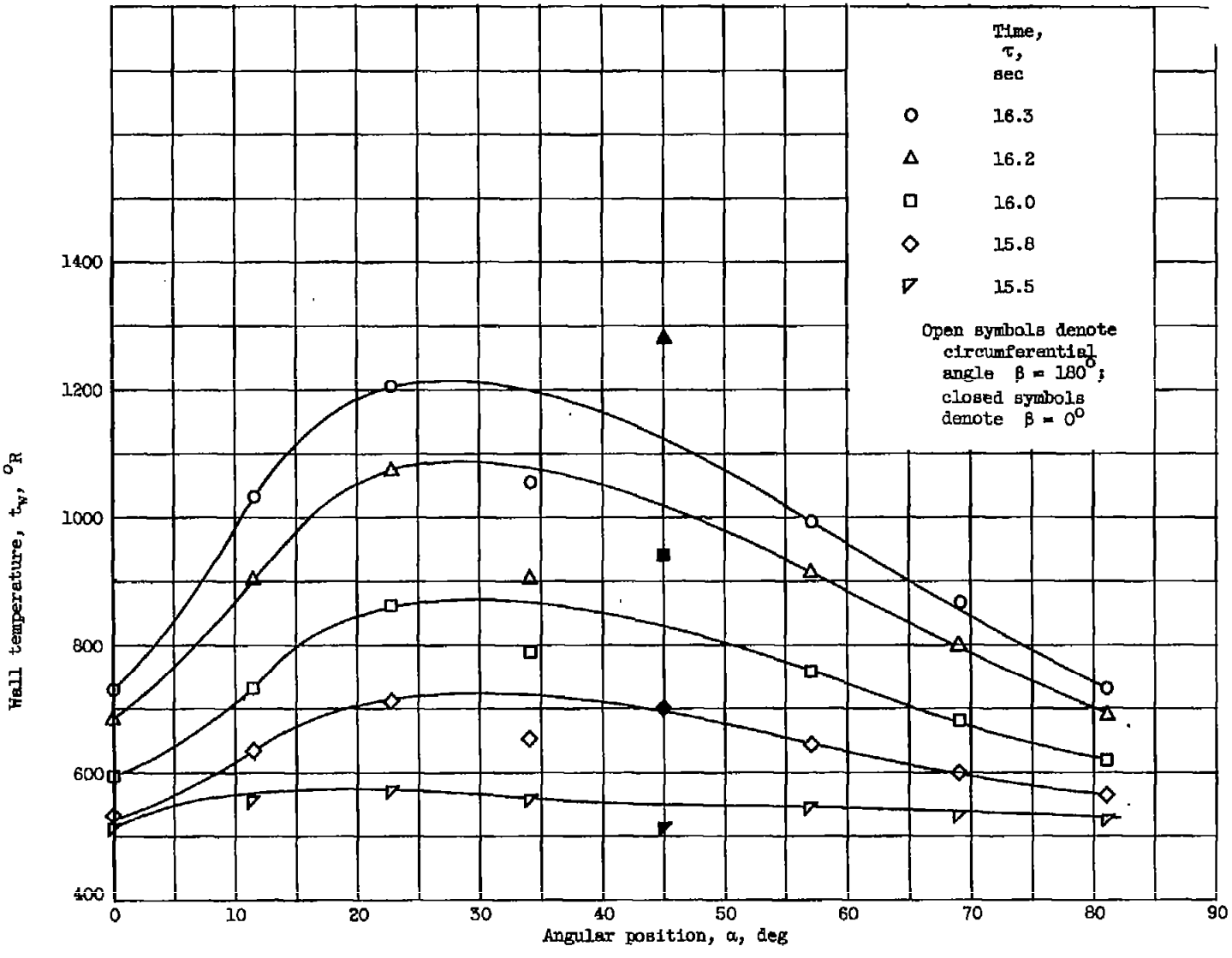

Figure 14. - Temperature profiles on hemisphere.

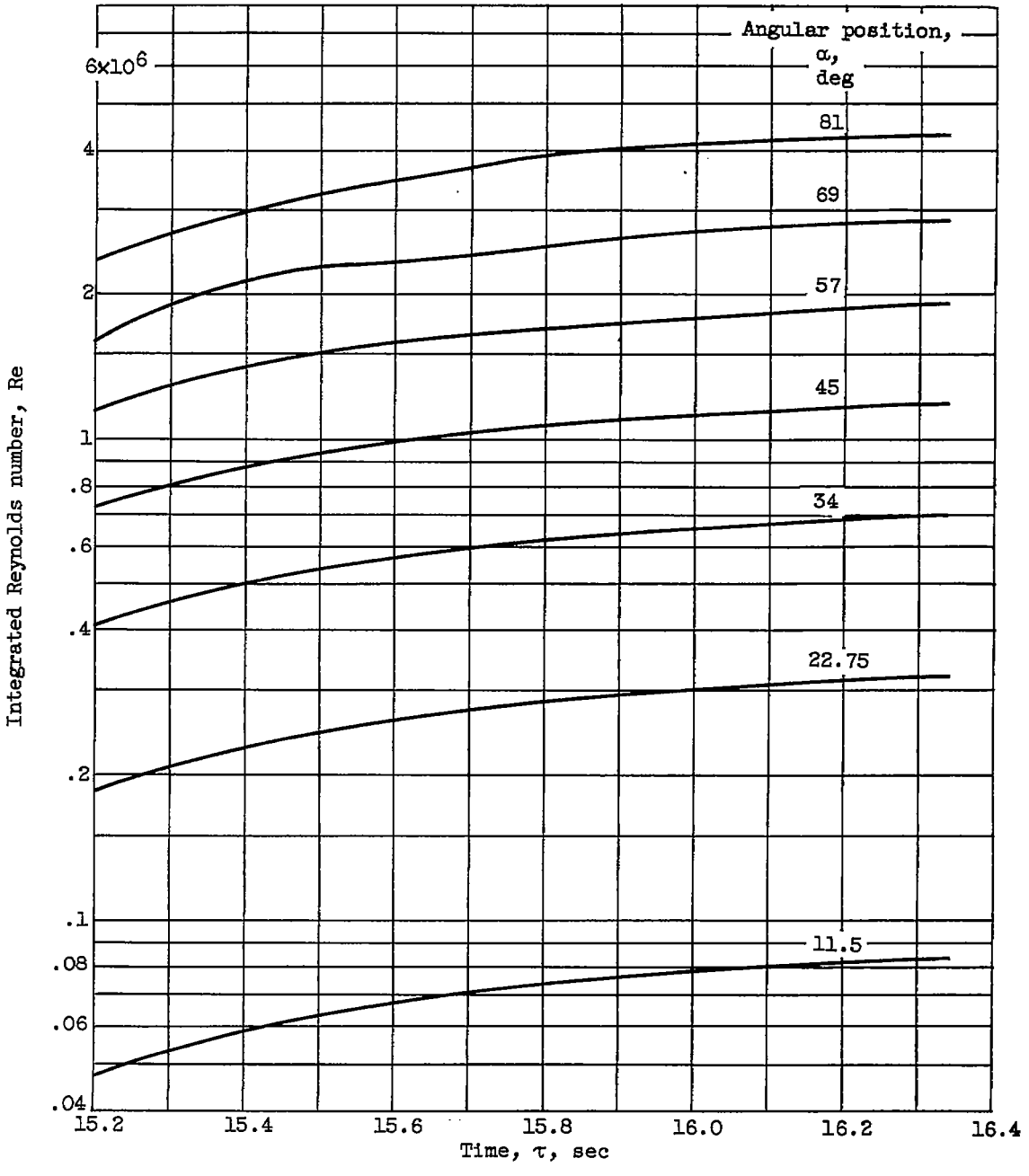

Figure 15. - Integrated Reynolds number plotted against time.

[redacted]

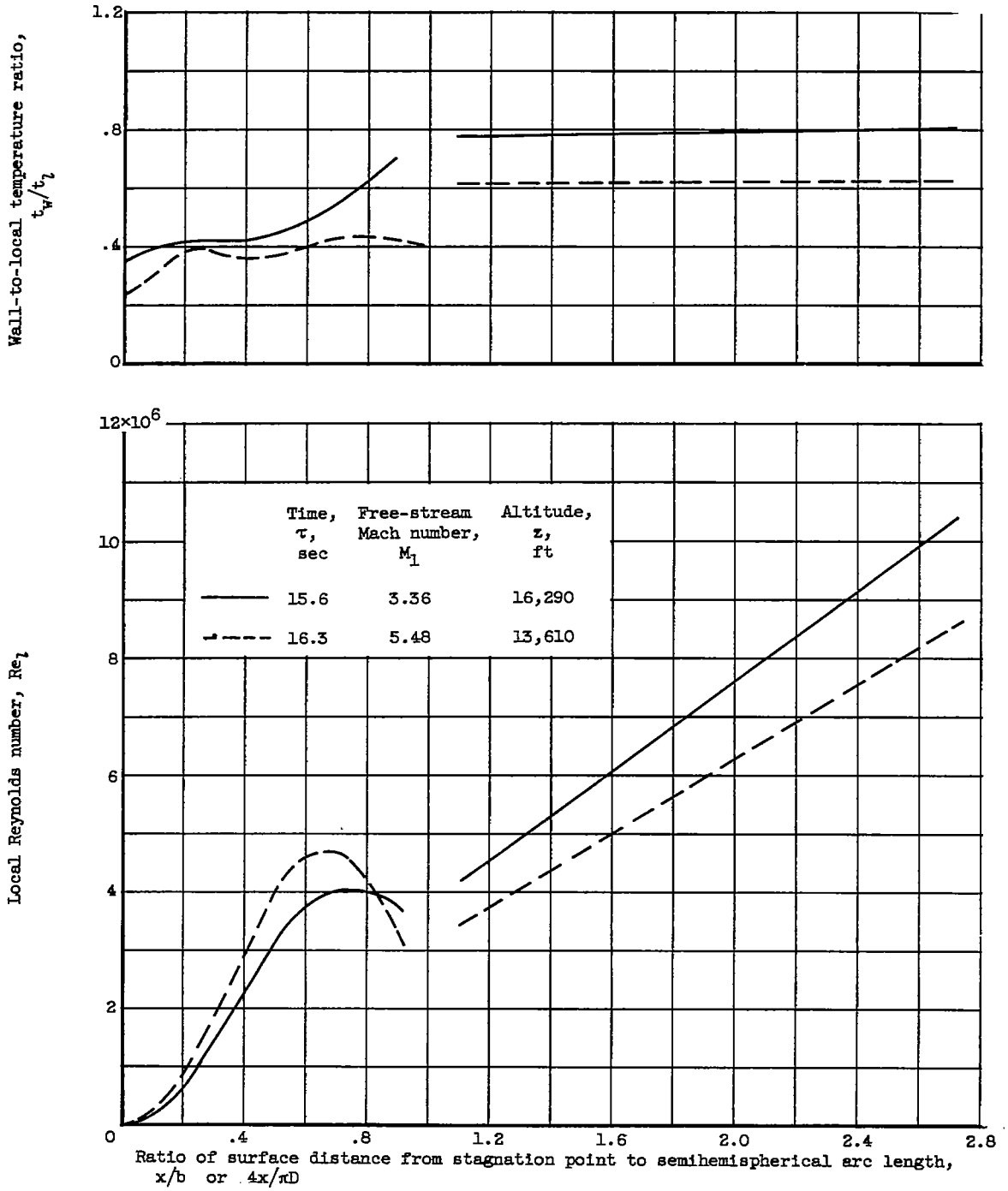

Figure 16. - Local Reynolds number and wall-to-local temperature ratio.